Article

Current Biology

Binocular Modulation of Monocular V1 Neurons

Highlights

- Monocular neurons in primate V1 layer 4C encode binocular inputs
- Firing rates of most monocular V1 neurons are suppressed under binocular viewing
- A neuron's ocularity and its binocular modulation are linearly related

Authors

Kacie Dougherty, Michele A. Cox, Jacob A. Westerberg, Alexander Maier

Correspondence

alex.maier@vanderbilt.edu

In Brief

Dougherty et al. evaluate to which degree neurons across V1 layers encode inputs to both eyes. So-called monocular neurons in the primary input layers of V1 modulate under binocular viewing, suggesting binocular signals arise at the input stage of V1.

Dougherty et al., 2019, Current Biology *29*, 381–391
February 4, 2019
https://doi.org/10.1016/j.cub.2018.12.004

CellPress

Current Biology
Article

Binocular Modulation of Monocular V1 Neurons

Kacie Dougherty,[1,3] Michele A. Cox,[2,3] Jacob A. Westerberg,[1] and Alexander Maier[1,4,*]
[1]Department of Psychology, College of Arts and Science, Vanderbilt Vision Research Center, Center for Integrative and Cognitive Neuroscience, Vanderbilt University, 2201 West End Avenue, Nashville, TN 37203, USA
[2]Center for Visual Science, University of Rochester, 500 Joseph C. Wilson Boulevard, Rochester, NY 14642, USA
[3]These authors contributed equally
[4]Lead Contact
*Correspondence: alex.maier@vanderbilt.edu
https://doi.org/10.1016/j.cub.2018.12.004

SUMMARY

In humans and other primates, sensory signals from each eye remain separated until they arrive in the primary visual cortex (V1), but their exact meeting point is unknown. In V1, some neurons respond to stimulation of only one eye (monocular neurons), while most neurons respond to stimulation of either eye (binocular neurons). The main input layers of V1 contain most of the monocular neurons while binocular neurons dominate the layers above and below. This observation has given rise to the idea that the two eyes' signals remain separate until they converge outside V1's input layers. Here, we show that, despite responding to only one eye, monocular neurons in all layers, including the input layers, of V1 discriminate between stimulation of their driving eye alone and stimulation of both eyes. Some monocular V1 neurons' responses were significantly enhanced, or facilitated, when both eyes were stimulated. Binocular facilitation within V1's input layers tended to occur at the onset of the visual response, which could be explained by converging thalamocortical inputs. However, most V1 monocular neurons were significantly reduced, or suppressed, to binocular stimulation. In contrast to facilitation, binocular suppression occurred several milliseconds following the onset of the visual response, suggesting that the bulk of binocular modulation involves cortical inhibition. These findings, combined, suggest that binocular signals arise at an earlier processing stage than previously appreciated, as even so-called monocular neurons in V1's input layers encode what is shown to both eyes.

INTRODUCTION

One of the most prominent features differentiating humans and other primates from their closest ancestors is that their eyes face to the front. One consequence of front-facing eyes is that their respective views largely overlap. Due to this overlap, primate brains need to combine the two eyes' views into a singular view [1, 2]. For this binocular combination to occur, the signals from the eyes need to meet at some point along the primary visual pathway. Although prior research has narrowed down possible locations underlying this convergence, we do not know the exact meeting point of the two eyes' signals.

Primate retinae do not receive feedback from the visual structures to which they project [3]. This absence of feedback suggests that the output of each eye is entirely separate from that of the other. Following visual transduction in the retina, the monocular signals from retinal ganglion cells mainly project to the lateral geniculate nucleus of the thalamus (LGN) [4]. For almost all primate LGN neurons, visually stimulating one eye leads to a response (dominant eye) while stimulating the other does not (non-dominant or silent eye). In other words, stimulation of each eye separately evokes responses in two mutually exclusive groups of LGN neurons. This segregation of eye-specific responses within the LGN suggests that the formation of a binocular signal occurs at a subsequent stage of visual processing.

As the next step in the primary visual pathway, LGN neurons primarily project to the primary visual cortex (V1) [4]. Neighboring LGN neurons that respond to stimulation of the same eye tend to innervate the same neurons in V1 layer 4 (in primates termed layer 4C, or L4) [5]. In line with this connectivity, many L4 neurons do not respond when a stimulus is shown to one of the eyes [6, 7]. L4 neurons converge onto neurons in the layers above [8], and most V1 neurons outside of L4 respond to stimuli shown to both eyes [6]. These findings have led to the popular interpretation that the signals from each eye remain largely segregated in L4 of V1.

The prevailing model of binocular convergence builds on all of these findings by proposing that V1 neurons in superficial layers (L2/3) of V1 receive inputs from both L4 neurons that respond to one eye as well as from L4 neurons that respond to the other eye [5]. This model explains why most L2/3 neurons respond to either eye (to varying degrees). L2/3 neurons project to neurons in the lower layers (L5/6) of V1, which also respond to stimulation of either eye [4].

Notably, the model outlined above assigns no significant role to the fact that L4 neurons also receive inputs from other V1 neurons in addition to the inputs from the LGN [9, 10]. Yet, these intracortical connections raise the interesting possibility that even monocular L4 neurons can encode a de-segregated binocular signal. This situation could arise if the firing rates of monocular neurons change reliably when both eyes are stimulated simultaneously. In other words, even though stimuli shown to their non-dominant eye alone do not evoke responses, monocular neurons might systematically modulate responses when stimuli are

shown to both eyes simultaneously. Indeed, previous studies showed that some monocular V1 neurons are tuned for interocular disparity and thus sensitive to both eyes [11–13]. However, whether such neurons can also be found in L4 is unclear because prior experiments lacked appropriate laminar resolution.

Here, we use laminar neurophysiology to determine whether the signals from the two eyes remain fully segregated in L4 of V1. To do so, we examined the extent to which neurons across all layers of V1 are sensitive to one or both eyes. Specifically, we employed linear multielectrode arrays to record V1 laminar neural responses in macaques that viewed stimuli with one eye, the other eye, or both eyes simultaneously. We found that binocular neurons, which significantly responded to either eye (paired t test; $\alpha = 0.05$), comprised 78% of V1 neurons across all layers. In line with earlier work, we located the bulk of monocular neurons, which responded to only one eye (paired t test; $\alpha = 0.05$), to L4. Strikingly, we found that, although activated by only one eye, L4 monocular neurons responded significantly differently when both eyes were stimulated simultaneously. These findings suggest that, despite their name, monocular neurons in the primary input layers of V1 actually encode both eyes' views. Thus, binocular signals arise at an earlier processing stage than commonly thought.

RESULTS

In each session, we penetrated the *dura mater* over V1 with a linear multielectrode array and positioned the array so that its contacts spanned the depth of cortex (Figure S1A) [14–16]. Although we recorded extracellular voltages, we displayed visual stimuli through a mirror stereoscope to stimulate the eyes independently (Figure 1A, upper panel). After mapping the population receptive field (RF) location for the neurons under study (Figure S1B; see STAR Methods), we presented static sine-wave gratings over the RF location to the dominant eye of the neuron, the non-dominant eye, or both eyes (Figures 1A, lower panel, and 1B). Following data collection, we extracted spiking activity from the extracellular voltage measurements (see STAR Methods).

Responses of V1 Monocular Neurons Modulate during Binocular Stimulation

We collected visual responses for 290 neurons throughout all V1 layers across both animals (261 from monkey E48; 29 from monkey I34). Congruent with previous work [6, 7], stimulation of either eye led to a statistically significant response (paired t test; $\alpha = 0.05$) for the majority of V1 neurons (n = 226). Monocular neurons that significantly responded to only one eye (paired t test; $\alpha = 0.05$) made up just 22% of the population (n = 64).

For a subset of neurons in our sample, we also collected responses to congruent (dioptic) stimulation of both eyes simultaneously (n = 138; n = 127 from monkey E48). We reasoned that, if monocular neurons were truly sensitive to only one eye, their responses should not differ between stimulating their dominant eye (monocular stimulation) or stimulating both eyes at the same time (binocular stimulation). Instead, we found that monocular neurons showed a significant difference between binocular and monocular stimulation. Specifically, monocular neurons exhibited a smaller median response to binocular stimulation than to dominant-eye stimulation (n = 33; two-tailed Wilcoxon signed-rank test; p = 0.029; Figure 1C; Table 1). When we redefined monocular neurons using an even stricter criterion that excluded any neuron that showed a (nonsignificant) change from baseline for silent eye stimulation, we observed the same effect (n = 8; two-tailed Wilcoxon signed-rank test; p = 0.0078; Figure S2A). We verified that fixational eye movements did not affect this result (n = 33; two-tailed Wilcoxon signed-rank test; p = 0.0076; Figure S2B). These results combined suggest that monocular V1 neurons can encode a binocular signal.

The prevailing model of binocular processing suggests that signals from each eye remain separate in L4 of V1 before merging to a binocular signal in the layers above [5]. If the binocularly modulating monocular neurons that we recorded were all located outside L4, our results would fit the model. If, on the other hand, monocular neurons in L4 showed sensitivity to both eyes, the model would require revision. Given this distinction, we were curious to locate the binocularly modulating neurons within the laminar microcircuit.

Even Monocular Neurons in V1's Primary Input Layer Modulate under Binocular Viewing

We used current source density analysis (CSD) (see STAR Methods) to estimate the location of each neuron relative to the L4-L5 boundary (marked as 0.0 in Figure 1D). Congruent with previous work [5, 6], we found that L4 contained the majority of monocular neurons (0.0–0.5 mm above the L4-L5 boundary), with smaller fractions of monocular neurons in the layers above and below (Figure 1E).

Importantly, the waveforms of monocular neurons did not resemble the tri-phasic waveforms associated with axonal spikes [17], suggesting that we did not mistake LGN afferents for V1 neurons (Figure 1E). Furthermore, the characteristics of monocular neurons in our sample resembled those of previous reports in two important aspects: first, most binocular neurons (87%) that we recorded showed significant orientation tuning, whereas almost half of monocular neurons (42.4%) did not (Figure S3B) [6, 7, 18]. Second, monocular neurons had significantly higher baseline firing rates than binocular neurons (two-sample t test; $t_{288} = 4.83$; $p = 2.22 \times 10^{-6}$; Figure S3C), congruent with previous work [19] (but see [7]).

To determine whether monocular neurons in L4, specifically, modulated under binocular stimulation, we quantified the binocular modulation shown in Figure 1C for each monocular neuron. Specifically, we took the difference in firing rate between monocular (dominant eye) stimulation and binocular stimulation and divided by the sum of these two values. This analysis revealed that both eyes affected the activity of most L4 monocular neurons (Figure 1F; see also Table 1). Statistical hypothesis testing showed that 11 of the 17 monocular neurons inside L4 (64.7%) exhibited a significant response difference between monocular (dominant eye) stimulation and binocular stimulation (receiver operating characteristic [ROC] analysis, $\alpha = 0.05$; Figure S2C; STAR Methods). Outside of L4, 11 of the monocular neurons (68.8%) exhibited significant binocular modulation as well.

We were interested in investigating the relationship between orientation tuning and binocular modulation because prior work suggested that some L4 neurons receiving direct thalamic inputs show less selective orientation tuning than other V1

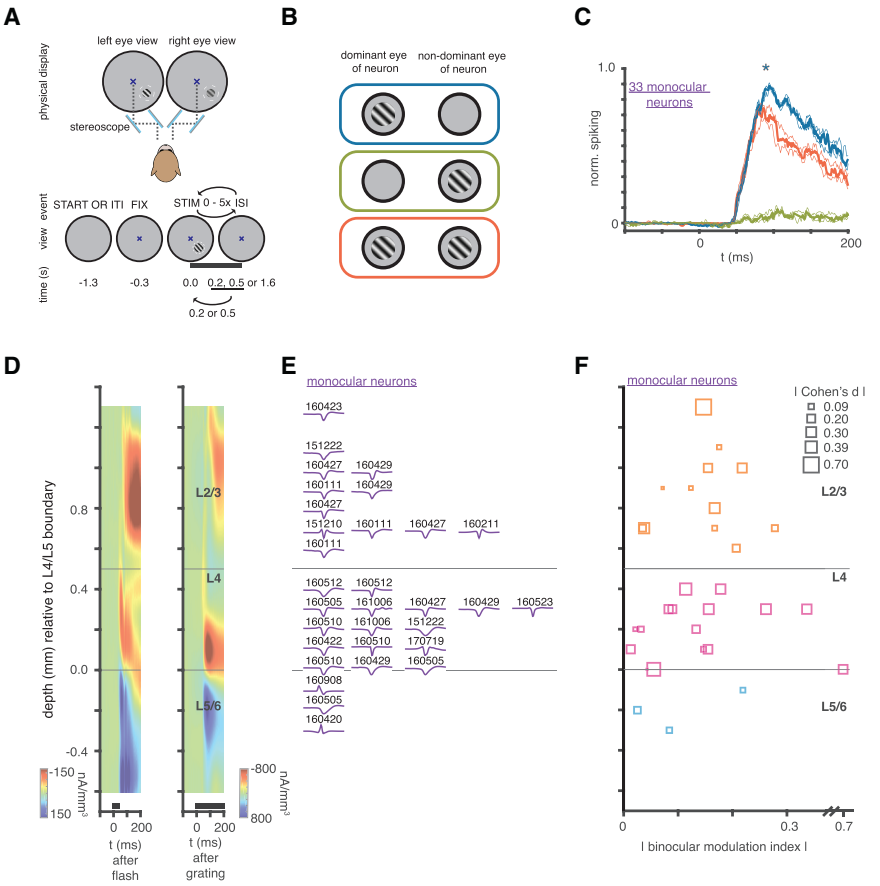

Figure 1. Responses of V1 Monocular Neurons Modulate During Binocular Stimulation

(A) Upper panel: experimental setup. Visual stimuli were presented to fixating macaque monkeys at the mapped receptive field location (white dashed circles) through a mirror stereoscope that consisted of two pairs of mirrors (top-down view; blue lines). The mirrors were angled in a way that each eye of the animal saw the left and right halves of the monitor, respectively (dashed black lines). Lower panel: schematic representation of the time series of stimulus presentation. Animals were rewarded for fixating on a central screen location while grating stimuli were presented in one or both eyes (see STAR Methods for details).

(B) On every stimulus presentation, a sine-wave grating was presented over the RF location to either the dominant eye of the neuron (blue), non-dominant eye (green), or both eyes (orange). Eye dominance was determined by statistically comparing the responses to stimulation of the left eye and right for each neuron (see STAR Methods).

(C) Median normalized spiking responses of monocular V1 neurons to the dominant eye (blue), both eyes (orange), and the non-dominant eye (green). Binocular stimulation significantly altered the monocular neurons' responses compared to stimulation of their dominant eye (two-tailed Wilcoxon signed-rank; $p = 0.029$; $n = 33$). Responses to the non-dominant eye alone were non-significant at $\alpha = 0.05$. Thin lines represent the 25% and 75% confidence limits on the median (chosen to account for the fact that the data were not normally distributed).

(D) Left panel: mean CSD (baseline-corrected, smoothed, and interpolated) response to a full-field white flash ($n = 33$ penetrations; both animals). Right panel: same as left panel for the response to a sine-wave grating presented at the RF location ($n = 45$ penetrations; both animals). Current sinks, which are linked to excitatory synaptic activity, are indicated in red. Current sources, which are caused by passive return currents, are shown in blue. 0 mm marks the L4-L5 border, as estimated by the bottom of the initial current sink that is evoked by the geniculo-cortical volley of activation (see STAR Methods). Gray horizontal lines mark the estimated boundaries of L4.

(E) Average spike waveforms for the monocular neurons shown in (C) at their relative position of cortical depth. Numbers indicate date of collection. Note that (C) includes two more neurons that were collected without laminar resolution (see Results for details).

(F) Magnitude of binocular modulation across cortical depth for neurons shown in (E). Marker size indicates rectified Cohen's d for each monocular neuron.

See also Figures S2, S3, and S4.

neurons [6]. Due to the experimental time limitations that come with working with awake animals, we were only able to reliably determine the orientation tuning for five L4 monocular neurons. Four of these neurons showed a significant effect for orientation (ANOVA; $p < 0.05$). Three neurons of those four neurons also showed a significant effect of binocular modulation (ROC analysis; $\alpha = 0.05$). Importantly, the un-tuned, monocular L4 neuron also showed significant binocular modulation (Figure S3A). Thus, stimulation of both eyes affects even un-tuned, monocular L4 neurons.

Binocular Modulation of V1 Monocular Neurons Is Both Suppressive and Facilitatory

Visual inspection of Figure 1C suggests that, across the population, binocular stimulation suppresses responses of V1 monocular neurons compared to dominant eye stimulation alone. We wondered how many (if any) individual monocular neurons show either no binocular suppression or enhanced (facilitated) responses during binocular stimulation. To answer this question, we rank ordered all monocular neurons from most facilitated to most suppressed (Figure 2A). This analysis revealed two distinct groups of binocularly modulating neurons: the first group decreased firing rates during binocular stimulation (binocularly suppressed neurons) and comprised over two-thirds of monocular neurons. The remaining one-third of monocular neurons increased firing rates during binocular stimulation (binocularly facilitated neurons).

The mean response across the binocularly suppressed neurons showed significant modulation (one-tailed Wilcoxon signed-rank test; $p = 1.44 \times 10^{-5}$; Figure 2B). Individual testing of binocularly suppressed neurons revealed that more than 80% (19/23) of these monocular neurons significantly reduced their activity upon binocular stimulation ($p < 0.05$; ROC analysis; see also Table 1). The mean response across the binocularly facilitated neurons showed significant enhancement under binocular stimulation (one-tailed Wilcoxon signed-rank; $p = 9.77 \times 10^{-4}$; Figure 2C). Testing on an individual neuron basis revealed that about half (4/10) of these neurons enhanced

Table 1. Fraction of Neurons with Significant Binocular Response Modulation at High Contrasts; ROC Analysis with Sliding 10-ms Windows; $\alpha = 0.05$

	15 Consecutive, Significant Windows	10 Consecutive, Significant Windows	20 Consecutive, Significant Windows
Binocular neurons	80/105	84/105	76/105
Monocular neurons	22/33	23/33	20/33
Suppressed monocular neurons	18/23	19/23	18/23
Facilitated monocular neurons	4/10	4/10	2/10
Liberal group of monocular neurons	33/50	34/50	31/50
Liberal group of suppressed monocular neurons	23/31	24/31	23/31
Liberal group of facilitated monocular neurons	10/20	10/20	8/20

their spiking significantly when both eyes were stimulated rather than their dominant eye alone (ROC analysis; Table 1).

We also repeated this comparison for a more liberally defined group of monocular neurons (one-tailed t test; $p > 0.01$). Using this liberal criterion yielded a larger sample size ($n = 51$) at the expense of including neurons that showed a minimal response to the non-dominant eye. Nonetheless, this liberally defined group yielded comparable results to those shown in Figures 2B and 2C (Figure S4C, one-tailed Wilcoxon signed-rank, $p = 6.17 \times 10^{-7}$, $n = 31$; Figure S4D, one-tailed Wilcoxon signed rank, $p = 4.78 \times 10^{-5}$, $n = 20$).

Psychophysical studies have shown that binocular combination differs at varying contrast levels [20, 21]. We therefore wondered whether stimulus contrast affects the binocular modulation of monocular neurons. To test for the impact of stimulus contrast, we recorded the responses of a subsample of monocular neurons to binocular stimuli presented at several contrast levels (see Table S1 for contrast levels and N). Specifically, we either did not display a stimulus (monocular conditions) or showed a high-contrast grating (binocular conditions) to the non-dominant eye. We then paired these conditions with stimuli of varying contrast in the dominant eye.

For both binocularly suppressed and facilitated monocular neurons, only high-contrast stimulation of the dominant eye resulted in significant binocular modulation (Figure 2D, one-tailed Wilcoxon signed-rank test, $p = 2.15 \times 10^{-5}$, Bonferroni corrected for multiple comparisons; Figure 2E, one-tailed Wilcoxon signed-rank test, $p = 9.77 \times 10^{-4}$, Bonferroni corrected for multiple comparisons). These results suggest that monocular V1 neurons modulate their firing rates at relatively high visual contrast levels only, congruent with the psychophysical observation that binocular combination differs fundamentally between high- and low-contrast levels.

Temporal Dynamics of Binocular Suppression Implies Intracortical Processing

What could cause the binocular modulation of L4 neurons described above? One possibility is that some L4 neurons receive convergent inputs from LGN afferents carrying signals from both eyes [22]. If this mechanism were involved, the difference between the overall visual response onset and the binocular modulation (effect) onset of L4 neurons would be small. Alternatively, monocular neurons may receive indirect inputs from the other eye either via lateral connections within L4 or via interlaminar connections that connect L4 cells to neurons in other layers. Both these mechanisms would involve more synapses and thus more processing time.

Given the rationale outlined above, we decided to compare visual response onsets and binocular modulation onsets of monocular neurons in L2/3, L4, and L5/6 (STAR Methods; see Figures S4A and S4B for the effect of binocular stimulation on binocular neurons). Congruent with the canonical microcircuit model [10], we found that L4 neurons tended to respond to visual stimulation before L2/3 neurons, followed by L5/6 neurons (L4, 42.1 ms; L2/3, 45.2 ms; L5/6, 46.4 ms; Figure 3A). As expected, binocular modulation significantly trailed the visual response by several milliseconds (median response onset: 50 ms; median binocular modulation onset: 62 ms; one-tailed Wilcoxon rank sum; $p = 2.01 \times 10^{-17}$). Interestingly, binocular modulation tended to occur first among L2/3 neurons, followed by L4 neurons and L5/6 neurons (L2/3, 47.6 ms; L4, 50.1 ms; L5/6, 54.7 ms; Figure 3B). This observation suggests that the bulk of binocular modulation of L4 neurons occurs following binocular processing outside V1's primary input layers.

L4 Binocular Facilitation Occurs Earlier Than Binocular Suppression

The above analyses suggest that, under binocular stimulation, most L4 neurons modulate via lateral connections within L4 or connections between L4 and L2/3 or L5/6. However, inspecting the data on a neuron-by-neuron basis revealed that some L4 neurons, including some monocular neurons, showed a more rapid onset of binocular modulation that virtually coincides with sensory activation (Figure 3C). One possible mechanism for this early L4 binocular modulation is that LGN afferents carrying signals from each eye converge onto L4 neurons. It is conceivable that the functional impact of some LGN afferents associated with the non-dominant eye might not be strong enough to drive a spiking response on their own but may nonetheless be effective enough to modulate responses to the dominant eye. As LGN inputs to L4 are excitatory [23], the result should be a rapid onset of facilitatory binocular modulation.

Indeed, we found that most of the facilitated monocular neurons were located in granular L4 (7/10). Furthermore, binocularly facilitated L4 neurons tended to modulate earlier than binocularly suppressed L4 neurons (Figure 3D). In other words, facilitatory binocular modulation by and large precedes suppressive binocular modulation in L4 (one-tailed Wilcoxon rank sum; $p = 0.16$).

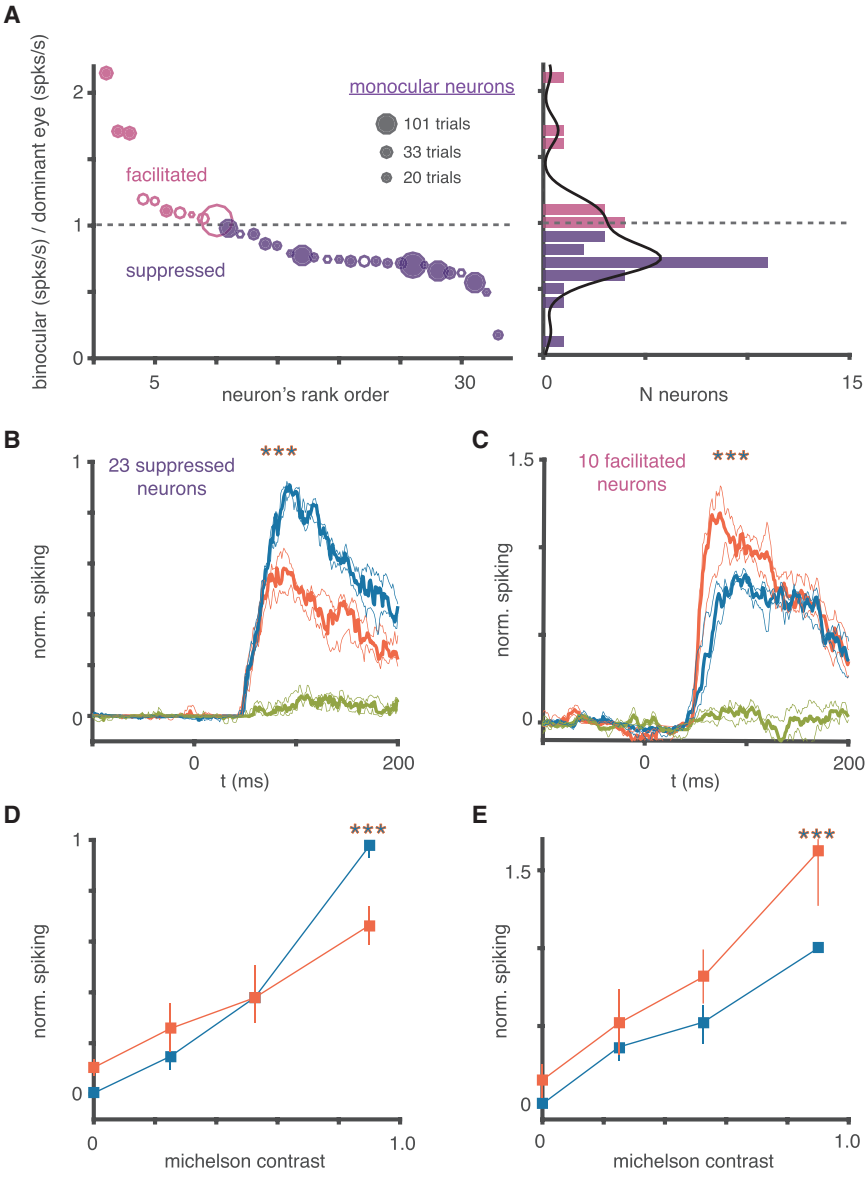

Figure 2. Binocular Modulation Is Both Suppressive and Facilitatory

(A) Left panel: rank ordering of monocular neurons from most facilitated to most suppressed, using the ratio of their binocular response to their dominant eye response. Solid circles indicate neurons with significant binocular modulation based on ROC analysis (α = 0.05 for 15 or more consecutive 10-ms sliding windows). Facilitated neurons that respond more when both eyes are stimulated are shown in pink. Suppressed neurons that reduce their response during binocular stimulation are shown in purple. Dashed horizontal line demarcates equal responses during monocular and binocular stimulation. Circle size indicates trial number. Right panel: histogram of the data shown to the left, with a kernel density estimate superimposed in black.

(B) Median normalized responses of *suppressed* monocular neurons that reduced firing rates during binocular stimulation (responses to the dominant eye are indicated in blue, to the non-dominant eye in green, and to both eyes in orange). Their population response to binocular stimulation differed significantly from monocular stimulation (one-tailed Wilcoxon signed-rank; $p = 1.44 \times 10^{-5}$; n = 23). All conventions are as in Figure 1C. Response to the non-dominant eye was non-significant at α = 0.05.

(C) Same as (B) for *facilitated* monocular neurons that increased spiking during binocular stimulation. Their population response under binocular stimulation was significantly greater than for stimulating their dominant eye alone (one-tailed Wilcoxon signed rank; $p = 9.77 \times 10^{-4}$; n = 10).

(D) Mean normalized contrast responses for suppressed monocular neurons during exclusive dominant eye stimulation (blue, non-dominant eye at 0.0 contrast) and binocular stimulation (orange, non-dominant eye at 0.8 or greater contrast). All contrast values and sample sizes are detailed in Table S1. Error bars represent 90% confidence limits. When the contrast of the stimulus in the dominant eye equal was 0.8 or greater, neurons were significantly suppressed (one-tailed Wilcoxon signed-rank test; $p = 2.15 \times 10^{-5}$; Bonferroni corrected for multiple comparisons). Differences at all other contrast levels were not significant.

(E) Same as (D) for facilitated monocular neurons. When the contrast of the stimulus in the dominant eye equal was 0.8 or greater, binocular stimulation resulted in significantly greater spiking responses than when stimulating the dominant eye alone (one-tailed Wilcoxon signed-rank test; $p = 9.77 \times 10^{-4}$; Bonferroni corrected for multiple comparisons).

See also Figure S4.

A Neuron's Degree of Ocular Preference Predicts Its Degree of Binocular Modulation

We next wondered how the above findings relate to the well-documented V1 phenomenon of ocular dominance [6, 18], which describes neuronal preferences for one eye over the other eye. Given that most monocular neurons are suppressed under binocular stimulation, is it that there is a systematic relationship between ocularity and the direction of binocular modulation? Or might this effect apply only to the monocular neuron population, with varied binocular modulation for all other (binocular) neurons? To answer this question, we estimated ocular dominance by computing an ocularity index for all single neurons and multiunits (see STAR Methods; see Figures S1C and S1D and [6, 18, 24] for the variance of ocular dominance across cortical depth). An ocularity index value of −1 corresponds to neurons exclusively driven through the ipsilateral eye, a value of 1 corresponds to neurons driven exclusively through the contralateral eye, and a value of 0 corresponds to neurons driven equally through either eye.

Our sample spanned the entire index range of ocular dominance (Figure 4A). Across the neuronal population, the spread of ocular dominance resembled a normal distribution (chi-square goodness of fit; $\chi^2 = 9.64$; d.f. = 7; p = 0.21; Figure 4B). We repeated this analysis for multiunits (see STAR Methods), as

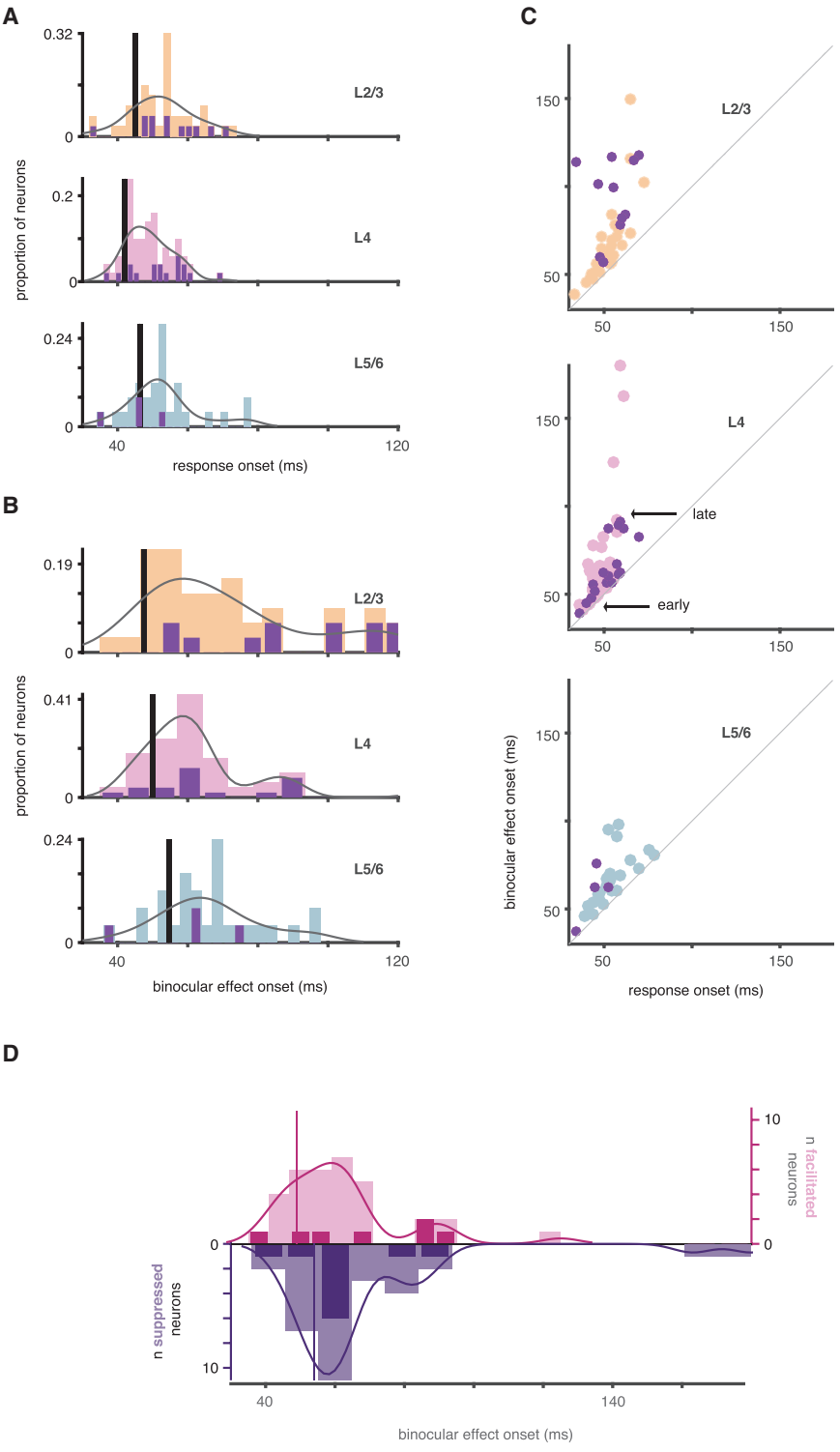

Figure 3. Binocular Modulation Tends to First Occur Outside of the Primary Input Layers

(A) Visual response onset distributions for L2/3, L4, and L5/6 neurons. Colored histograms encompass all neurons within each laminar compartment. Overlaid purple bars highlight the monocular neurons. Gray lines are kernel density fits. Black vertical lines indicate 75%-to-maximum of fitted distributions.

(B) Binocular modulation onset distributions for L2/3, L4, and L5/6 neurons. Conventions are as in (A).

(C) Visual response onset versus binocular modulation onset for L2/3, L4, and L5/6 neurons. Purple markers indicate monocular neurons. Gray line represents unity line.

(D) L4 binocular facilitation precedes binocular suppression. Histogram of binocular modulation onset for suppressed L4 neurons (top, n = 32) and facilitated L4 neurons (bottom, n = 34). The darker bars represent suppressed monocular neurons (n = 10) and facilitated monocular neurons (n = 7), respectively. Solid lines represent kernel density. Vertical lines represent the 0.25 quantile for the L4 facilitated neurons (purple, 49 ms) and L4 suppressed neurons (54 ms), respectively.

these data provide a larger sample. Multiunit responses reflect the activity of neurons up to 350 μm away from the electrode contact [25], which can bridge across ocular dominance columns [26]. Given this coarser spatial sampling, we expected multiunits to exhibit a stronger bias toward binocular responses. Indeed, multiunits had lower mean rectified ocularity indices than single neurons (one-tailed two-sample t test; $p = 1.98 \times 10^{-25}$; $t_{1285} = 10.58$). Like the single-neuron population, multiunit ocular dominance also resembled a normal distribution (chi-square goodness of fit; $\chi^2 = 3.95$; d.f. = 7; $p = 0.79$; Figure 4C), suggesting that the mode of ocular dominance in V1 is an equal response to either eye.

Given this wide range of ocular dominance among our sample of V1 neurons, we wondered whether ocular dominance and binocular modulation were systematically related. To test for this relationship, we calculated a binocular modulation index, as described for Figure 1F, that quantifies both the strength and direction of binocular modulation (see STAR Methods). We then assessed whether a neuron's ocular dominance had any explanatory power for the neuron's binocular modulation.

Interestingly, and largely congruent with the findings described above, we found a significant correlation between the binocular modulation index and the rectified ocularity index ($p = 0.0011$; $r = -0.275$; $r^2 = 0.0756$; Figure 4D). This significant correlation suggests that the more a neuron prefers one eye over the other, the more binocular stimulation suppresses that neuron. We observed the same significant correlation for our larger sample of multiunits ($p = 1.29 \times 10^{-18}$; $r = -0.348$; $r^2 = 0.121$; Figure 4E), across all V1 layers

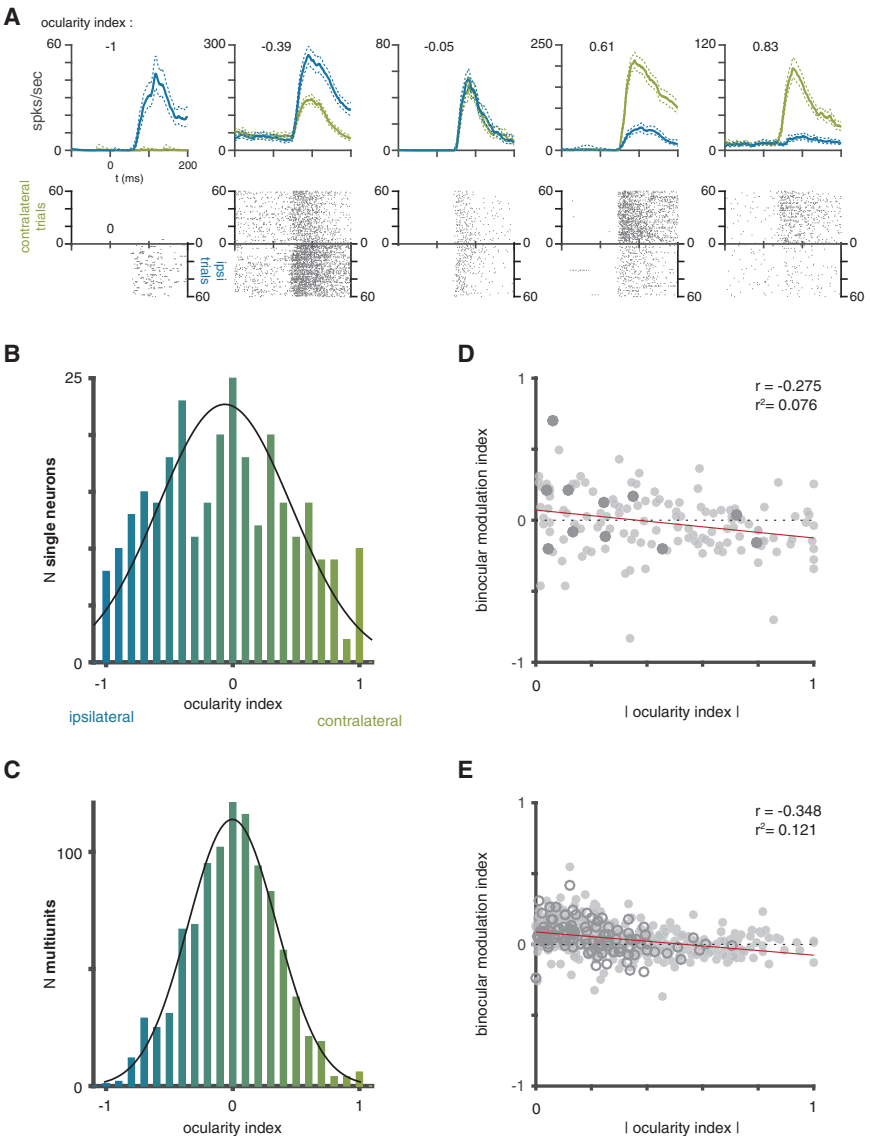

Figure 4. Ocular Dominance Correlates with Binocular Modulation

(A) Responses for five example neurons of varying ocular dominance. Top row: mean spike density functions (thick lines) with 95% confidence intervals (thin lines). Responses to the contralateral eye are shown in green. Responses to the ipsilateral eye are shown in blue. Corresponding raster plots (60 randomly selected trials for each condition) are shown below. The resulting ocularity index (see STAR Methods) for each neuron is shown in the top left corner.

(B) Histogram overlaid with fitted Gaussian (black line) for the ocularity indices of all recorded single neurons (n = 290; chi-square goodness of fit; χ^2 = 9.64; d.f. = 7; p = 0.21; H_0 = underlying distribution is normal).

(C) Same as (B) for all multiunits recorded in our sample (n = 997). Fit is Gaussian (chi-square goodness of fit; χ^2 = 3.95; d.f. = 7; p = 0.79; H_0 = underlying distribution is normal).

(D) Binocular modulation as a function of ocularity across all of the neurons that we measured under binocular stimulation (n = 138). Higher ocularity indices indicate greater preference for one eye over the other. Lower binocular modulation indices indicate more response suppression during binocular stimulation. The solid red line represents a linear regression using least squares (p = 0.0011; r = −0.275; r^2 = 0.0756). The dashed line indicates the expected relationship if there were no systematic response differences between a monocular neuron's ocular bias and its binocular modulation. Darker markers represent neurons from monkey I34.

(E) Rectified ocularity index versus binocular modulation index across all multiunits with binocular data (n = 602). The solid red line represents a linear regression using least squares (p = 1.29 × 10^{-18}; r = −0.348; r^2 = 0.121). All conventions are as in (D).

See also Figures S1 and S5.

(L2/3, p = 6.20 × 10^{-10}, r = −0.418, r^2 = 0.174; L4, p = 1.19 × 10^{-10}, r = −0.438, r^2 = 0.192; L5/6, p = 0.005, r = −0.197, r^2 = 0.039; Figure S5).

DISCUSSION

This study demonstrates that almost all primate V1 neurons, including those in layer 4C, encode sensory signals from both eyes. We found that there are both facilitatory as well as suppressive effects of binocular stimulation among monocular neurons. The temporal profile of binocular modulation suggests that at least some form of binocular facilitation in L4 could arise from additive synaptic activation of neurons that directly receive inputs from both eyes. In contrast, binocular suppression seems to depend on one or more steps of intracortical processing. These findings suggest that established models of binocular processing that segregate monocular signals in L4 (Figure 5A) [5] need revision (Figure 5B). Moreover, we found that the more a V1 neuron responds to one eye compared to the other, the more binocular stimulation suppresses its responses. This result is significant because several theoretical models on binocular vision rest on the idea that activation of a monocular neuron's non-dominant eye can reduce its response [21, 27–29], yet until now, empirical support has been lacking.

Relation to Prior Work

The findings reported here parallel similar observations in cat area 17 [30]. This analogy is interesting because binocular processing in cats differs significantly from primates. For example, eye-specific terminations of LGN neurons in L4 of visual cortex in monkeys are more segregated in monkeys than in cats [5, 31]. Moreover, cat LGN features anatomical connections between monocular layers that are either absent or less prominent in primates [32–34]. Accordingly, responses of the vast majority of cat LGN cells modulate under binocular stimulation, whereas only a small minority of LGN neurons in the macaque seem to be

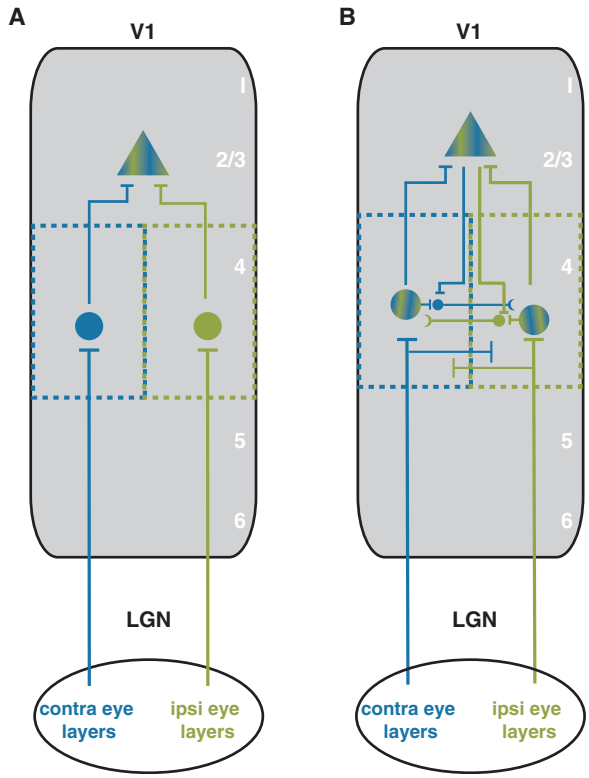

Figure 5. Schematic Model for the Formation of Binocular Signals in V1

(A) Earlier models of binocular processing purported that monocular signals remain segregated in L4 of V1. Formation of a binocular signal occurs outside of L4.

(B) New, modified model that incorporates the results from this study. Given that most V1 monocular neurons in L4 are sensitive to both eyes, binocular signals exist in V1's input layer. Some of this sensitivity could arise from (1) excitatory, convergent inputs from the lateral geniculate nucleus (LGN) onto L4 neurons, as well as (2) lateral connections within L4 or (3) interlaminar connections.

sensitive to both eyes (see [35] for more extensive discussion). Our results suggest that despite these species differences, monocular neurons in primary visual cortex of both cats and monkeys exhibit binocular modulation.

Given these analogous results, we decided to use the previously published cat data to compute a statistical power analysis. The result showed that, for the reported effect size and estimated variance, 80% power could be achieved with 11 monocular neurons, suggesting that our sample size—though small—offered satisfactory degrees of freedom [30].

Previous work in primates suggested that most V1 neurons are sensitive to interocular disparity [36]. Our finding that virtually all V1 neurons—including monocular neurons in L4—carry binocular signals is consistent with, and corroborate, this idea. Several primate studies also quantified the fraction of binocular and monocular primate V1 cells [37, 38], and some considered ocularity across cortical depth [6, 24]. Several of these studies used a scale to rate the extent to which one eye or the other drives neurons [24, 37, 39]. This ocular dominance scale consists of 7 distinct groups, with groups 1 and 7 corresponding to neurons driven exclusively by the contra- and ipsilateral eyes, respectively [6]. Group 4 corresponds to neurons driven equally through both eyes. Using this technique, some authors reported distributions appearing Gaussian [39], matching our finding, while others reported more uniform distributions [37]. The subjective nature of the rating system as well as potential differences in the laminar position of sampled neurons might explain some of this variance. Importantly, though, previous studies and the data reported here agree that monocular neurons make up only a small fraction of V1 neurons [40].

Binocular Modulation and Disparity Tuning

We did not systematically test our recorded neurons for interocular disparity tuning but instead presented all of our binocular stimuli at zero disparity exclusively. It is possible that stimulation of both eyes using interocular disparity might reveal that even some of the monocular neurons in our sample that did not show a significant effect of binocular modulation are nonetheless sensitive to both eyes. In other words, it is conceivable that binocular stimuli shown at disparities other than zero modulate monocular neurons that do not modulate at zero disparity. Indeed, previous studies in both cats and monkeys found disparity tuning among monocular V1 neurons [11–13]. Our findings expand on these studies by demonstrating that a large fraction of monocular neurons V1 that are sensitive to both eyes are located in the primary input layers (L4) and that binocular modulation and ocularity are linearly related.

Possible Role of the LGN

Another important consideration is that binocular convergence may initiate in the LGN. Specifically, monocular LGN neurons might modulate under binocular stimulation and imprint this response pattern onto their projection targets in L4 of V1. Indeed, binocular modulation occurs in cat LGN (see [35] for review). It is unclear whether this binocular modulation results from feedback from V1 [32, 41–43]. However, the finding of extensive binocular modulation in cat LGN could not be replicated in primates [44], which suggests that the two species differ substantially in their functional organization of binocular integration [45]. Future work may determine the degree of binocular modulation in primate LGN as well as the role of corticofugal feedback in its implementation. It is also worth noting that a small fraction of primate LGN neurons can be driven through either eye [46, 47]. Whether local neural interactions or cortical feedback cause these binocular responses is unknown. However, these binocular LGN cells make up less than 3% of all LGN neurons. Taken together, these observations suggest that the vast majority of geniculate inputs to L4 do not encode binocular signals in primates. Therefore, cortical activity is likely responsibly for most of the binocular modulation of monocular neurons reported here.

Possible Explanations for the Binocular Modulation of Monocular Neurons

The binocular response modulation of monocular neurons that we observed could arise through one of several mechanisms or a combination thereof.

One possibility is that V1 monocular neurons in L4 receive subthreshold inputs from their non-dominant eye. This is an intriguing

idea because several empirical and psychophysical studies suggest that monocular neurons interact at or before the point where monocular signals merge into a binocular signal [21, 48], and human fMRI corroborates this prediction [49]. Indeed, some geniculate projections to V1 L4 have been shown to bifurcate and innervate neighboring ocular dominance columns [22]. These axons might form—possibly less potent—connections with neurons in ocular dominance columns of the other eye, thus leading to binocular convergence at the thalamo-cortical synapse. However, this kind of connectivity could only explain binocular facilitation and not binocular suppression, because geniculate projections to V1 are exclusively excitatory. Indeed, L4 binocularly facilitated neurons tended to modulate earlier than L4 binocularly suppressed neurons. This finding is congruent with the idea that some L4 neurons receive weak excitatory input from their non-dominant eye (Figure 5B). However, binocular facilitation occurred for only a fraction of monocular V1 neurons, which means that axonal convergence in L4 cannot explain the majority of binocular modulation that we observed.

A second possibility is that binocular modulation occurs by lateral interactions among L4 neurons, such as interneurons that cross ocular dominance columns [50, 51]. This connectivity would allow for cross-talk between the signals of each eye [9, 44]. The idea that L4 interneurons are involved in L4 binocular modulation agrees with our finding that the predominant form of binocular modulation among monocular V1 neurons is suppressive. In the same vein, the fact that suppressive binocular modulation trailed the initial visually evoked sensory response by several milliseconds provides further evidence for the idea that intracortical processing is involved in the bulk of L4 binocular modulation (Figure 5B).

A third possibility is that binocular modulation occurs via excitatory and inhibitory neurons from other layers onto L4 neurons. Such interlaminar connections might feed binocular signals back to these monocular cells in L4 [52, 53]. In this case, intracellular combination of monocular inputs from either eye first occurs outside of L4. The resulting binocular signals are then fed back to L4, causing binocular modulation. This possibility can explain binocular suppression, as well as the delayed onset of binocular modulation for suppressed neurons. This idea gains even further traction given our finding that binocular modulation in L2/3 slightly preceded binocular modulation in L4. It thus seems plausible that L2/3 neurons cause some of the binocular suppression among L4 monocular neurons (Figure 5B).

STAR★METHODS

Detailed methods are provided in the online version of this paper and include the following:

SUPPLEMENTAL INFORMATION

Supplemental Information includes five figures and one table and can be found with this article online at https://doi.org/10.1016/j.cub.2018.12.004.

ACKNOWLEDGMENTS

The authors would like to thank S. Amemori, Dr. T. Apple, M. Feurtado, K. George-Durrett, Dr. A. Graybiel, N. Halper, P. Henry, M. Johnson, Dr. C. Jones, M. Maddox, L. McIntosh, Dr. A. Newton, J. Parker, M. Schall, C. Thompson, K. Torab, Dr. C. Subraveti, B. Williams, R. Williams, and Dr. W. Zinke for technical advice and assistance. We thank Dr. B. Cumming, Dr. P. Martin, B.M. Carlson, and N. Valov for comments on an earlier version of this manuscript. This work was supported by a research grant from the National Eye Institute (1R01EY027402-02), as well as training grant T32EY007135 (to K.D. and J.A.W.) and core grant P30EY008126 from the National Eye Institute. The authors are grateful to Dr. D. Calkins and support from the Vanderbilt Vision Research Center. MRI scans were performed at the Vanderbilt University Institute of Imaging Science (VUIIS) Center for Human Imaging on a 3T scanner supported by NIH grant 1 S10OD021771 01. A.M. is supported by a research grant from the Whitehall Foundation, a Career Starter grant by the Knights Templar Eye Foundation, and a fellowship from the Alfred P. Sloan Foundation.

AUTHOR CONTRIBUTIONS

Conceptualization, K.D., M.A.C., and A.M.; Methodology, K.D. and M.A.C.; Investigation, K.D., M.A.C., and J.A.W.; Formal Analysis, K.D. and M.A.C.; Writing – Original Draft, K.D. and A.M.; Writing – Review and Editing, K.D., M.A.C., J.A.W., and A.M.

DECLARATION OF INTERESTS

The authors declare no competing interests.

Received: August 10, 2018
Revised: November 5, 2018
Accepted: December 5, 2018
Published: January 17, 2019

REFERENCES

1. Parker, A.J., and Cumming, B.G. (2001). Cortical mechanisms of binocular stereoscopic vision. Prog. Brain Res. *134*, 205–216.
2. Ohzawa, I., DeAngelis, G.C., and Freeman, R.D. (1997). Encoding of binocular disparity by complex cells in the cat's visual cortex. J. Neurophysiol. *77*, 2879–2909.
3. Repérant, J., Miceli, D., Vesselkin, N.P., and Molotchnikoff, S. (1989). The centrifugal visual system of vertebrates: a century-old search reviewed. Int. Rev. Cytol. *118*, 115–171.
4. Casagrande, V.A., and Boyd, J.D. (1996). The neural architecture of binocular vision. Eye (Lond.) *10*, 153–160.
5. Hubel, D.H., and Wiesel, T.N. (1972). Laminar and columnar distribution of geniculo-cortical fibers in the macaque monkey. J. Comp. Neurol. *146*, 421–450.
6. Hubel, D.H., and Wiesel, T.N. (1968). Receptive fields and functional architecture of monkey striate cortex. J. Physiol. *195*, 215–243.
7. Blasdel, G.G., and Fitzpatrick, D. (1984). Physiological organization of layer 4 in macaque striate cortex. J. Neurosci. *4*, 880–895.
8. Douglas, R.J., Martin, K.A.C., and Whitteridge, D. (1989). A canonical microcircuit for neocortex. Neural Comput. *1*, 480–488.

9. Ahmed, B., Anderson, J.C., Douglas, R.J., Martin, K.A., and Nelson, J.C. (1994). Polyneuronal innervation of spiny stellate neurons in cat visual cortex. J. Comp. Neurol. *341*, 39–49.
10. Binzegger, T., Douglas, R.J., and Martin, K.A. (2004). A quantitative map of the circuit of cat primary visual cortex. J. Neurosci. *24*, 8441–8453.
11. Ohzawa, I., and Freeman, R.D. (1986). The binocular organization of simple cells in the cat's visual cortex. J. Neurophysiol. *56*, 221–242.
12. Prince, S.J., Pointon, A.D., Cumming, B.G., and Parker, A.J. (2002). Quantitative analysis of the responses of V1 neurons to horizontal disparity in dynamic random-dot stereograms. J. Neurophysiol. *87*, 191–208.
13. Read, J.C., and Cumming, B.G. (2004). Ocular dominance predicts neither strength nor class of disparity selectivity with random-dot stimuli in primate V1. J. Neurophysiol. *91*, 1271–1281.
14. Maier, A., Adams, G.K., Aura, C., and Leopold, D.A. (2010). Distinct superficial and deep laminar domains of activity in the visual cortex during rest and stimulation. Front. Syst. Neurosci. *4*, 31.
15. Dougherty, K., Cox, M.A., Ninomiya, T., Leopold, D.A., and Maier, A. (2017). Ongoing alpha activity in V1 regulates visually driven spiking responses. Cereb. Cortex *27*, 1113–1124.
16. Cox, M.A., Dougherty, K., Adams, G.K., Reavis, E.A., Westerberg, J.A., Moore, B.S., Leopold, D.A., and Maier, A. (2017). Spiking suppression precedes cued attentional enhancement of neural responses in primary visual cortex. Cereb. Cortex. Published online November 23, 2017.. https://doi.org/10.1093/cercor/bhx305
17. Lemon, R., and Prochazka, A. (1984). Methods for Neuronal Recording in Conscious Animals. IBRO Handbook Series (Chichester, New York: Wiley), p. 162.
18. Hubel, D.H., and Wiesel, T.N. (1977). Ferrier lecture. Functional architecture of macaque monkey visual cortex. Proc. R. Soc. Lond. B Biol. Sci. *198*, 1–59.
19. Snodderly, D.M., and Gur, M. (1995). Organization of striate cortex of alert, trained monkeys (Macaca fascicularis): ongoing activity, stimulus selectivity, and widths of receptive field activating regions. J. Neurophysiol. *74*, 2100–2125.
20. Legge, G.E., and Rubin, G.S. (1981). Binocular interactions in suprathreshold contrast perception. Percept. Psychophys. *30*, 49–61.
21. Ding, J., and Sperling, G. (2006). A gain-control theory of binocular combination. Proc. Natl. Acad. Sci. USA *103*, 1141–1146.
22. Blasdel, G.G., and Lund, J.S. (1983). Termination of afferent axons in macaque striate cortex. J. Neurosci. *3*, 1389–1413.
23. da Costa, N.M., and Martin, K.A.C. (2011). How thalamus connects to spiny stellate cells in the cat's visual cortex. J. Neurosci. *31*, 2925–2937.
24. Schiller, P.H., Finlay, B.L., and Volman, S.F. (1976). Quantitative studies of single-cell properties in monkey striate cortex. II. Orientation specificity and ocular dominance. J. Neurophysiol. *39*, 1320–1333.
25. Mineault, P.J., Zanos, T.P., and Pack, C.C. (2013). Local field potentials reflect multiple spatial scales in V4. Front. Comput. Neurosci. *7*, 21.
26. Horton, J.C., and Hocking, D.R. (1996). Intrinsic variability of ocular dominance column periodicity in normal macaque monkeys. J. Neurosci. *16*, 7228–7239.
27. Blake, R. (1989). A neural theory of binocular rivalry. Psychol. Rev. *96*, 145–167.
28. Read, J.C., Parker, A.J., and Cumming, B.G. (2002). A simple model accounts for the response of disparity-tuned V1 neurons to anticorrelated images. Vis. Neurosci. *19*, 735–753.
29. Said, C.P., and Heeger, D.J. (2013). A model of binocular rivalry and cross-orientation suppression. PLoS Comput. Biol. *9*, e1002991.
30. Kato, H., Bishop, P.O., and Orban, G.A. (1981). Binocular interaction on monocularly discharged lateral geniculate and striate neurons in the cat. J. Neurophysiol. *46*, 932–951.
31. Wiesel, T.N., Hubel, D.H., and Lam, D.M. (1974). Autoradiographic demonstration of ocular-dominance columns in the monkey striate cortex by means of transneuronal transport. Brain Res. *79*, 273–279.
32. Sanderson, K.J., Bishop, P.O., and Darian-Smith, I. (1971). The properties of the binocular receptive fields of lateral geniculate neurons. Exp. Brain Res. *13*, 178–207.
33. Hayhow, W.R. (1958). The cytoarchitecture of the lateral geniculate body in the cat in relation to the distribution of crossed and uncrossed optic fibers. J. Comp. Neurol. *110*, 1–63.
34. Guillery, R.W., and Colonnier, M. (1970). Synaptic patterns in the dorsal lateral geniculate nucleus of the monkey. Z. Zellforsch. Mikrosk. Anat. *103*, 90–108.
35. Dougherty, K., Schmid, M.C., and Maier, A. (2018). Binocular response modulation in the lateral geniculate nucleus. J. Comp. Neurol. Published online February 23, 2018. https://doi.org/10.1002/cne.24417.
36. Poggio, G.F., and Fischer, B. (1977). Binocular interaction and depth sensitivity in striate and prestriate cortex of behaving rhesus monkey. J. Neurophysiol. *40*, 1392–1405.
37. Kiorpes, L., Kiper, D.C., O'Keefe, L.P., Cavanaugh, J.R., and Movshon, J.A. (1998). Neuronal correlates of amblyopia in the visual cortex of macaque monkeys with experimental strabismus and anisometropia. J. Neurosci. *18*, 6411–6424.
38. Macknik, S.L., and Martinez-Conde, S. (2004). Dichoptic visual masking reveals that early binocular neurons exhibit weak interocular suppression: implications for binocular vision and visual awareness. J. Cogn. Neurosci. *16*, 1049–1059.
39. Parker, A.J. (2007). Binocular depth perception and the cerebral cortex. Nat. Rev. Neurosci. *8*, 379–391.
40. Baker, F.H., Grigg, P., and von Noorden, G.K. (1974). Effects of visual deprivation and strabismus on the response of neurons in the visual cortex of the monkey, including studies on the striate and prestriate cortex in the normal animal. Brain Res. *66*, 185–208.
41. Singer, W. (1970). Inhibitory binocular interaction in the lateral geniculate body of the cat. Brain Res. *18*, 165–170.
42. Schmielau, F., and Singer, W. (1977). The role of visual cortex for binocular interactions in the cat lateral geniculate nucleus. Brain Res. *120*, 354–361.
43. Varela, F.J., and Singer, W. (1987). Neuronal dynamics in the visual corticothalamic pathway revealed through binocular rivalry. Exp. Brain Res. *66*, 10–20.
44. Katz, L.C., Gilbert, C.D., and Wiesel, T.N. (1989). Local circuits and ocular dominance columns in monkey striate cortex. J. Neurosci. *9*, 1389–1399.
45. Rodieck, R.W., and Dreher, B. (1979). Visual suppression from nondominant eye in the lateral geniculate nucleus: a comparison of cat and monkey. Exp. Brain Res. *35*, 465–477.
46. Cheong, S.K., Tailby, C., Solomon, S.G., and Martin, P.R. (2013). Cortical-like receptive fields in the lateral geniculate nucleus of marmoset monkeys. J. Neurosci. *33*, 6864–6876.
47. Zeater, N., Cheong, S.K., Solomon, S.G., Dreher, B., and Martin, P.R. (2015). Binocular visual responses in the primate lateral geniculate nucleus. Curr. Biol. *25*, 3190–3195.
48. Truchard, A.M., Ohzawa, I., and Freeman, R.D. (2000). Contrast gain control in the visual cortex: monocular versus binocular mechanisms. J. Neurosci. *20*, 3017–3032.
49. Moradi, F., and Heeger, D.J. (2009). Inter-ocular contrast normalization in human visual cortex. J. Vis. *9*, 1–22.
50. Buzás, P., Eysel, U.T., Adorján, P., and Kisvárday, Z.F. (2001). Axonal topography of cortical basket cells in relation to orientation, direction, and ocular dominance maps. J. Comp. Neurol. *437*, 259–285.
51. Martin, K.A.C., Somogyi, P., and Whitteridge, D. (1983). Physiological and morphological properties of identified basket cells in the cat's visual cortex. Exp. Brain Res. *50*, 193–200.
52. Gilbert, C.D., and Wiesel, T.N. (1989). Columnar specificity of intrinsic horizontal and corticocortical connections in cat visual cortex. J. Neurosci. *9*, 2432–2442.

53. Wiser, A.K., and Callaway, E.M. (1997). Ocular dominance columns and local projections of layer 6 pyramidal neurons in macaque primary visual cortex. Vis. Neurosci. *14*, 241–251.

54. Pachitariu, M., Steinmetz, N.A., Kadir, S.N., Carandini, M., and Harris, K.D. (2016). Kilosort: realtime spike-sorting for extracellular electrophysiology with hundreds of channels. bioRxiv. https://doi.org/10.1101/061481.

55. Otero-Millan, J., Castro, J.L.A., Macknik, S.L., and Martinez-Conde, S. (2014). Unsupervised clustering method to detect microsaccades. J. Vis. *14*, 18.

56. Asaad, W.F., Santhanam, N., McClellan, S., and Freedman, D.J. (2013). High-performance execution of psychophysical tasks with complex visual stimuli in MATLAB. J. Neurophysiol. *109*, 249–260.

57. Sayer, R.J., Friedlander, M.J., and Redman, S.J. (1990). The time course and amplitude of EPSPs evoked at synapses between pairs of CA3/CA1 neurons in the hippocampal slice. J. Neurosci. *10*, 826–836.

58. Hanes, D.P., Thompson, K.G., and Schall, J.D. (1995). Relationship of presaccadic activity in frontal eye field and supplementary eye field to saccade initiation in macaque: Poisson spike train analysis. Exp. Brain Res. *103*, 85–96.

59. Nicholson, C., and Freeman, J.A. (1975). Theory of current source-density analysis and determination of conductivity tensor for anuran cerebellum. J. Neurophysiol. *38*, 356–368.

60. Logothetis, N.K., Kayser, C., and Oeltermann, A. (2007). In vivo measurement of cortical impedance spectrum in monkeys: implications for signal propagation. Neuron *55*, 809–823.

61. Maier, A., Logothetis, N.K., and Leopold, D.A. (2007). Context-dependent perceptual modulation of single neurons in primate visual cortex. Proc. Natl. Acad. Sci. USA *104*, 5620–5625.

62. Maier, A., Wilke, M., Aura, C., Zhu, C., Ye, F.Q., and Leopold, D.A. (2008). Divergence of fMRI and neural signals in V1 during perceptual suppression in the awake monkey. Nat. Neurosci. *11*, 1193–1200.

63. Mitzdorf, U., and Singer, W. (1977). Laminar segregation of afferents to lateral geniculate nucleus of the cat: an analysis of current source density. J. Neurophysiol. *40*, 1227–1244.

64. Schroeder, C.E., Mehta, A.D., and Givre, S.J. (1998). A spatiotemporal profile of visual system activation revealed by current source density analysis in the awake macaque. Cereb. Cortex *8*, 575–592.

65. Maier, A., Aura, C.J., and Leopold, D.A. (2011). Infragranular sources of sustained local field potential responses in macaque primary visual cortex. J. Neurosci. *31*, 1971–1980.

66. Godlove, D.C., Maier, A., Woodman, G.F., and Schall, J.D. (2014). Microcircuitry of agranular frontal cortex: testing the generality of the canonical cortical microcircuit. J. Neurosci. *34*, 5355–5369.

67. Spaak, E., Bonnefond, M., Maier, A., Leopold, D.A., and Jensen, O. (2012). Layer-specific entrainment of γ-band neural activity by the α rhythm in monkey visual cortex. Curr. Biol. *22*, 2313–2318.

68. van Kerkoerle, T., Self, M.W., Dagnino, B., Gariel-Mathis, M.A., Poort, J., van der Togt, C., and Roelfsema, P.R. (2014). Alpha and gamma oscillations characterize feedback and feedforward processing in monkey visual cortex. Proc. Natl. Acad. Sci. USA *111*, 14332–14341.

69. Hansen, B.J., Chelaru, M.I., and Dragoi, V. (2012). Correlated variability in laminar cortical circuits. Neuron *76*, 590–602.

70. Ninomiya, T., Dougherty, K., Godlove, D.C., Schall, J.D., and Maier, A. (2015). Microcircuitry of agranular frontal cortex: contrasting laminar connectivity between occipital and frontal areas. J. Neurophysiol. *113*, 3242–3255.

71. Cox, M.A., Schmid, M.C., Peters, A.J., Saunders, R.C., Leopold, D.A., and Maier, A. (2013). Receptive field focus of visual area V4 neurons determines responses to illusory surfaces. Proc. Natl. Acad. Sci. USA *110*, 17095–17100.

72. Green, D.M., and Swets, J.A. (1966). Signal Detection Theory and Psychophysics (New York: Wiley), p. 455.

STAR★METHODS

KEY RESOURCES TABLE

REAGENT or RESOURCE	SOURCE	IDENTIFIER
Experimental Models: Organisms/Strains		
Bonnet macaque (*Macaca radiata*)	Wake Forest University, North Carolina, USA	N/A
Software and Algorithms		
MATLAB, 2012-2014 and 2016A	MathWorks	https://www.mathworks.com
MonkeyLogic	David Freedman, University of Chicago; Wael Assad, Brown University	http://www.brown.edu/Research/monkeylogic/
KiloSort	[54]	https://github.com/cortex-lab/KiloSort
Microsaccade Detection	[55]	http://smc.neuralcorrelate.com/sw/microsaccade-detection/
Other		
Vector Array	NeuroNexus	http://neuronexus.com/products/neural-probes/
U-Probe, V-Probe	Plexon	https://plexon.com/
Recording equipment	Blackrock Microsystems	http://blackrockmicro.com/
Eye Link II Eye Tracker	SR Research	https://www.sr-research.com/
Cold mirrors	Edmund Optics	https://www.edmundoptics.com/
Data Acquisition Board PCI-6229	National Instruments	http://www.ni.com/en-us.html
Eye-tracking software	SensoMotoric Instruments	https://www.smivision.com/
Eye camera	MRC Systems GmbH	www.mrc-systems.de
Photodiode	OSI Optoelectronics	http://www.osioptoelectronics.com/
Ceramic screws	Thomas Recording	https://www.thomasrecording.com/
Dental Acrylic	Lang Dental Manufacturing	http://www.orthodonticproductsonline.com/buyers-guide/listing/lang-dental-manufacturing-co-inc/
Plastic Recording Chamber	Crist Instrument; custom-made	http://www.cristinstrument.com/; Vanderbilt University

CONTACT FOR REAGENT AND RESOURCE SHARING

Further information and requests for resources and reagents should be directed to and will be fulfilled by the Lead Contact, Alexander Maier (alex.maier@vanderbilt.edu).

EXPERIMENTAL MODEL AND SUBJECT DETAILS

Two adult monkeys (*Macaca radiata,* one female*)* were used in this study. Both animals were pair-housed. Both animals were on a 12-hour light-dark cycle, and all experimental procedures were carried out in the daytime. Each monkey received nutrient-rich, primate-specific food pellets twice a day, along with fresh produce and other forms of environmental enrichment at least five times a week. All procedures followed regulations by the Association for the Assessment and Accreditation of Laboratory Animal Care (AAALAC), Vanderbilt University's Institutional Animal Care and Use Committee (IACUC) and National Institutes of Health (NIH) guidelines.

METHOD DETAILS

Surgical Procedures

Prior to data collection, each monkey was implanted with a custom-designed plastic head holder and a plastic recording chamber (Crist Instruments) in two separate surgeries under sterile conditions. The animals were administered isoflurane anesthesia (1.5%–2.0%). Vital signs, including blood pressure, heart rate, SpO_2, CO_2, respiratory rate and body temperature were continuously monitored throughout the whole procedure. During surgery, the head holder or the recording chamber was attached to the skull using transcranial ceramic screws (Thomas Recording) and self-curing dental acrylic (Lang Dental Manufacturing). A craniotomy was performed over the perifoveal visual field representation of primary visual cortex (V1) in each monkey concurrent with the positioning of the recording chamber. Each monkey was given analgesics and antibiotics, and closely observed by researchers, facility veterinarians and animal care staff for at least three days following surgery.

Data Acquisition and Pre-Processing

During each recording session, a linear multielectrode array (U-Probe, Plexon, or Vector Array, NeuroNexus) with either 24 or 32 contacts of 0.1 mm inter-contact spacing was carefully inserted into V1. Extracellular voltage fluctuations (0.5 Hz – 30 kHz) were recorded inside an electromagnetic radio frequency-shielded booth. These signals were amplified, filtered and digitized using a 128-channel Cerebus Neural Signal Processing System (NSP; Blackrock Microsystems). Both a broadband (0.3 Hz – 7.5 kHz) signal sampled at 30 kHz and a low frequency-dominated signal (0.3 Hz – 500 Hz) sampled at 1 kHz was saved for offline analysis. The NSP also recorded the output of a photodiode signal (OSI Optoelectronics) placed on the monitor to track stimulus-related events at 30 kHz. The NSP further digitized the output of the optical eye tracking system (EyeLink II, SR Research or SensoMotoric Instruments) at 1 kHz, as well as digital event markers sent from the behavioral control system (MonkeyLogic [56]. Both the photodiode signal and event markers were used to align the neural data with visual and behavioral events.

All neurophysiological signals, except for local field potentials (LFP), were extracted offline from the digitized broadband signal using custom written code in MATLAB (2016a; The Mathworks). LFP was extracted from the low frequency-dominated signal described above.

We extracted multiunits by applying a time-varying threshold to the envelope of the broadband signal, and saved all time points where the signal envelope exceeded a preset threshold. Specifically, we first lowpass-filtered the 30 kHz-sampled voltage signal at 5 kHz using a second order Butterworth filter. We then downsampled the signal by a factor of 3. Next, we high pass-filtered the signal at 1 kHz cut-off with a second-order Butterworth filter. Finally, we rectified the resulting data. To compute the signal envelope, we downsampled the signal by a factor of 3. To compute a threshold, we smoothed the signal by convolving the data with a 1 s boxcar function and then multiplied the result by 2.2. To recover temporal information, we extracted ± 0.3 ms of data from the original signal for each time point where the envelope exceeded the threshold. We then adjusted these time points to correspond to the point of maximum slope within this window.

For laminar alignment (see below), we used an analog multiunit signal that was computed by high-pass filtering the broadband signal at 750 Hz with a fourth-order Butterworth filter, followed by a full-wave rectification step.

We extracted single neurons with KiloSort, an open-source unsupervised machine-learning algorithm for spike-sorting [54], using the default parameters for sorting and cluster merging. We extracted ± 1 ms of data around each KiloSort'ed spike time from the original broadband signal for each simultaneously recorded electrode contact. We then averaged across impulses to create a spatiotemporal map of the spike waveform (time x electrode contacts). The region of the spatiotemporal waveform map that exceeded ± 30% of maximum modulus had to span fewer than 3 electrode contacts (0.3 mm) and 0.9 ms to be included in the study. Neurons that met these criteria were localized to the electrode contact where they evoked the largest amplitude.

Spike rates were downsampled to 1 kHz. For each neuron, spike times were converted to a time-varying signal (spike density function) using 0 to represent time points without a spike and 1 for time points where a spike was detected. This time-varying signal was then convolved using a Poisson distribution resembling a postsynaptic potential [57], with the spike rate (R) computed at time (t):

$$R(t) = \left[1 - \exp\left(-\frac{t}{\tau_g}\right)\right] * \left[\exp\left(-\frac{t}{\tau_d}\right)\right]$$

where τ_g and τ_d are the time constants for growth and decay, respectively. Values of 1 and 20 for τ_g and τ_d respectively were used based on a previous study [58]. After convolution, the signal was multiplied by the sampling frequency to convert units to spikes per second.

Current source density (CSD) analysis was performed on the LFP signal using an estimate of the second spatial derivative appropriate for electrodes with multiple contact points [59]:

$$CSD(t,c) = -\frac{\mathrm{x}(t,c-z) + \mathrm{x}(t,c+z) - 2\mathrm{x}(t,c)}{z^2}$$

where x is the extracellular voltage recorded in Volts at time t from an electrode contact at position c, and z is the electrode inter-contact distance (0.1 mm). In order to yield CSD in units of current per unit volume, the resulting CSD from the formula above was multiplied by 0.4 S/mm as an estimate of cortical conductivity [60].

Eye position was measured continuously using a commercially available eye tracker (see details below). Using the horizontal and vertical gaze position data, we extracted microsaccades using a previously published algorithm [55].

Visual Display

Stimuli were presented on a linearized CRT monitor with a refresh rate of either 60 Hz (resolution 1280 × 1024) or 85 Hz (resolution 1024 × 768). These visual stimuli were generated using custom-written code for MonkeyLogic [56] in MATLAB (R2012-2014, The MathWorks) on a PC (Dell, Windows 7 or Windows 10) with a NVIDIA graphics card. Animals viewed all stimuli through a custom-built mirror stereoscope that employed infrared-light passing cold mirrors (Edmund Optics). The animal, mirrors and monitor were positioned so that the animal's right eye viewed stimuli presented on the right side of the monitor and the animal's left eye viewed stimuli on the left side of the monitor. To prevent light scatter from one side of the monitor to the opposing eye, a black, non-reflective septum was placed between the monitor and the back side of the mirrors, effectively dividing the left and right sides of the apparatus.

Infrared-light sensitive cameras, placed directly behind the cold mirrors on the stereoscope, were used to track gaze position with commercially available eye tracking software (Eye Link II, SR Research). Gaze position was converted to an analog signal

and inputted to MonkeyLogic/MATLAB (NIDAQ PCI-6229) at 1 kHz. At the beginning of each recording session, the stereoscope was calibrated to facilitate binocular fusion of the left and right sides of the monitor using a behavioral task that relied on acquiring the same gaze position for corresponding locations on each side of the monitor [61, 62]. To further aid fusion, an oval aperture or set of intersecting circles in each corner was displayed at the edge of each half-screen.

Laminar Alignment and RF Mapping

For each penetration with the linear multielectrode array, CSD analysis was used to locate the boundary between L4 and L5. CSD analysis of visual responses to brief visual stimulation has been shown to reliably indicate the location of the primary geniculate input to V1 (in granular L4) by a distinct current sink that is thought to reflect the combined excitatory post-synaptic potentials of the initial retino-geniculate volley of activation [63, 64]. Lack of multiunit responses were used to identify electrode contacts that lie outside V1, either in the subdural space or the white matter below. We excluded contacts on the extreme ends of the array that did not exhibit a visual response. After removing these contacts, the location of the initial current sink was used to align and average data across electrode penetrations, resulting in 0.1 mm ± 0.05 mm resolution across the depth of V1 [14–16, 65–70].

For display, representations of CSD as a function of time and space were Gaussian-filtered (σ = 0.1), and interpolated across the spatial dimension. Electrode contacts were classified to be in supragranular, granular, or infragranular positions based on the CSD responses as well as neurophysiological criteria. These criteria included the power spectral density of the LFP across cortical depth, signal correlations of the LFP between all contact combinations, and stimulus-evoked analog multiunit responses. The supragranular-to-granular boundary is more challenging to define based on these criteria and was instead set to 0.5 mm above the granular to infragranular boundary.

Once the linear multielectrode array was appropriately positioned in cortex, a reverse correlation-like technique was used to map the RFs of the neurons under study. In each trial, the animals fixated while up to five circular Gabor-filtered static random noise patches appeared in sequence at pseudorandom locations within a pre-defined virtual grid of monitor locations. Each noise patch was displayed for 150 ms with an inter-stimulus interval of 150 ms. The size of each noise patch and the pre-defined grid varied between recording sessions. Typically, each session included a ''coarse'' mapping phase to determine the general location of the RF. We then used a subsequent ''fine'' mapping phase to map the precise location of the RF. Afterwards, we used 3D Receptive Field Matrices (RFMs) [71] to create a map of neuronal responses to different points in visual space for each electrode contact (see Figure S5A). For every multiunit or single neuron, we averaged the spiking response to each stimulus presentation across time, resulting in a single scalar value. We then converted these scalar values to units of z-score. We filled the retinotopic portion of the RFM corresponding to the stimulus location with the z-score for every presentation. This procedure produced a 3D matrix, with two dimensions representing vertical and horizontal visual space and a third dimension representing the response magnitude for each multiunit or neuron. We then averaged this third dimension to produce a spatial map of the mean response. We computed RF centers and extents by fitting an oval to the largest, contiguous patch of the spatial map that exceeded 1 z-score.

Monocular and Binocular Visual Stimulation

We trained each animal to fixate on a small (0.2 degrees of visual angle, dva) cross presented at the center of each eye's visual field. Animals held fixation for several (< 5) seconds while we presented stimuli in their perifoveal visual field. The results reported in this paper are based on data that come from three different paradigms, all with the same or similar conditions. For all neurons, we recorded responses to high contrast (0.8 or greater) sine-wave gratings at varied orientations presented to the left eye or right eye. For 138 neurons, we also recorded responses to high contrast sine-wave gratings at varied orientations presented to both eyes simultaneously. For fewer neurons (see Table S1), we recorded responses to sine-wave gratings where the contrast in the two eyes varied at several different levels. We presented all stimuli for at least 200 ms, and limited the data to the initial 200 ms of stimulus presentation for each neuron. Where data for multiple paradigms existed for one neuron, we concatenated data across the same conditions.

In one paradigm, animals fixated on a fixation cross for at least 300 ms before a sequence of up to five circular sinusoidal gratings appeared. Each grating was presented for at least 200 ms (46 sessions) or 500 ms (23 sessions) before an inter-stimulus interval of at least 200 ms. We presented the gratings randomly to either the left eye, right eye, or both eyes over the population RF location of the recorded neurons. The grating stimuli varied in orientation but always had a Michelson contrast above 0.8 (mode: 0.9) as well as constant spatial frequency (0.5-3 cycles/deg). If the animals successfully held fixation within a 1 dva radius around the fixation cross for the entire stimulus sequence, liquid juice reward was delivered. If the animals broke fixation or blinked, the trial was aborted and a short timeout (1-5 s) was given before the start of the next trial.

In the second paradigm, we used the same parameters, including stimulus timing. However, we presented the gratings at only one of two orientations (the neurons' estimated preferred orientation or the orientation orthogonal to this preferred orientation) and varied contrast of the gratings shown to each eye across trials (see Table S1). We determined the preferred orientation based on online analyses of the multiunit responses to sine-wave gratings of varying orientations. If preferred orientation varied across electrode contacts, we chose the preferred orientation shared by the most number of contacts.

In the third paradigm, the animals fixated for at least 300 ms before we presented gratings at the same orientation in both eyes (either the preferred or non-preferred orientation, as described for paradigm two) and varied contrast of the gratings shown to each eye across trials (see Table S1). Stimuli were shown for 1600 ms (12 sessions). If the animals successfully held fixation within a 1 dva radius around the fixation cross for the entire stimulus duration, liquid juice reward was delivered. If the animals broke fixation or blinked, the trial was aborted and a short timeout (1-5 s) was given before the start of the next trial.

MRI

Animals were anesthetized using the same procedure as outlined under Surgical Procedures. Anesthetized animals were placed inside a Philips Achieva 7T MRI scanner at the Vanderbilt University Institute of Imaging Science and remained anesthetized throughout the duration of the scan. Vital signs were monitored continuously. T1-weighted 3D MPRAGE scans were acquired with a 32-channel head coil equipped for SENSE imaging. Images were acquired using a 0.5 mm isotropic voxel resolution with the following parameters: repetition time (TR) 5 s, echo time (TE) 2.5 ms, flip angle 7°.

QUANTIFICATION AND STATISTICAL ANALYSIS

For a KiloSort'ed neuron or multiunit to be considered for additional analysis, it had to be located within the gray matter (see Laminar Alignment and RF Mapping). Moreover, the neuron or multiunit's mean initial response (40-100 ms) to the dominant eye (defined as the eye that yielded the highest mean spike rate between 40 ms and 140 ms when stimulated with a high contrast stimulus) had to exceed a maximum of 10 spikes per second. This response also had to be significantly larger than the fixation baseline (baseline window: −50-0 ms, paired t test, $p < 0.05$). Lastly, there had to be at least 12 successfully completed presentations of each monocular contralateral and monocular ipsilateral eye stimulation using the high contrast gratings.

To compute normalized spiking, we transformed the mean responses for each neuron to z-scores. Specifically, we first subtracted their baseline firing rate. Then, we divided this value by the difference between the maximum firing rate to stimulation of the dominant eye and the baseline firing rate. Similarly, we normalized contrast response data across conditions for each neuron by subtracting the baseline firing rate from the mean response at each contrast level. Then, we divided each resulting value by the difference between high contrast dominant eye stimulation and baseline firing.

All statistical hypothesis tests, including Wilcoxon signed-rank tests (one and two-sided), ANOVAs with post hoc Tukey HSD tests, Chi-square goodness of fit tests, and Pearson's correlation analysis, are fully described where used in RESULTS, FIGURE LEGENDS, and METHOD DETAILS. All reported confidence intervals were based on bootstrapping using 10,000 repetitions on the group statistic (mean or median) shown.

Neurons were included in the monocular category if they had a non-significant dominant eye response during the initial stimulation window (40 to 100 ms) relative to baseline (−50 to 0 ms) (one-tailed paired t test, $p < 0.05$). We re-categorized two neurons as binocular following visual inspection of average responses.

To quantify the relative amount of excitation by stimulation of the contralateral eye versus by that of the ipsilateral eye, we calculated an ocularity index for each unit:

$$ocularity\ index = \frac{contralateral\ eye\ response - ipsilateral\ eye\ response}{contralateral\ eye\ response + ipsilateral\ eye\ response},$$

where response was defined as the half-wave rectified, baseline-subtracted mean spike rate during the initial response period (40-140 ms). We calculated a binocular modulation index to assess the strength and direction of binocular modulation using the following formula:

$$-1 \times \frac{dominant\ eye\ response - binocular\ response}{dominant\ eye\ response + binocular\ reponse}.$$

We calculated response onset for each neuron using a custom algorithm. Briefly, we used the z-scored response to stimulation in the dominant eye to determine the first time point that exceeded a threshold while trending in positive direction. Specifically, we parceled the data into overlapping windows, whose length was defined as 3% of the maximum response time. We then defined a threshold as the mean response plus two standard deviations for the time between 15 ms before to 15 ms after stimulus onset. If the resulting threshold was lower than 0.05, it was set to 0.05. Criterion was met if 90% of data points within a window exceeded this threshold while 70% of data points trended positively. If no data point fit those criteria, we used the first time point that crossed threshold instead. We used the same algorithm to calculate the binocular effect onset, except that we ran the algorithm on the rectified difference between the median response across trials to the dominant eye and the median response to binocular stimulation.

In addition to group statistics, we used receiver-operating characteristics (ROC) analysis [72] to determine whether there was a significant difference between stimulation conditions at the single-neuron level. Specifically, for each neuron, we ran an ROC analysis with twelve thresholds using 10 ms bins of data, and a sliding window of 1 ms during the response period (20-190 ms). Statistical significance was determined by comparing the area under the curve to a bootstrapped distribution of area under the curve values computed on 10,000 repetitions of shuffled data. We counted the number of neurons in each defined group (monocular neurons, binocular neurons, etc.) with a 10, 15, or 20 consecutive significant windows (see Table 1). Wherever ROC analysis is reported in the text or figure legends, unless otherwise stated, a unit had to have 15 consecutive windows with $p < 0.05$ in order to be called significant. We show how the number of units marked as significant changes with different criteria in Table 1.

DATA AND SOFTWARE AVAILABILITY

Code used for analyses in this paper are available upon request from the corresponding author.

Current Biology, Volume *29*

Supplemental Information

Binocular Modulation of Monocular V1 Neurons

Kacie Dougherty, Michele A. Cox, Jacob A. Westerberg, and Alexander Maier

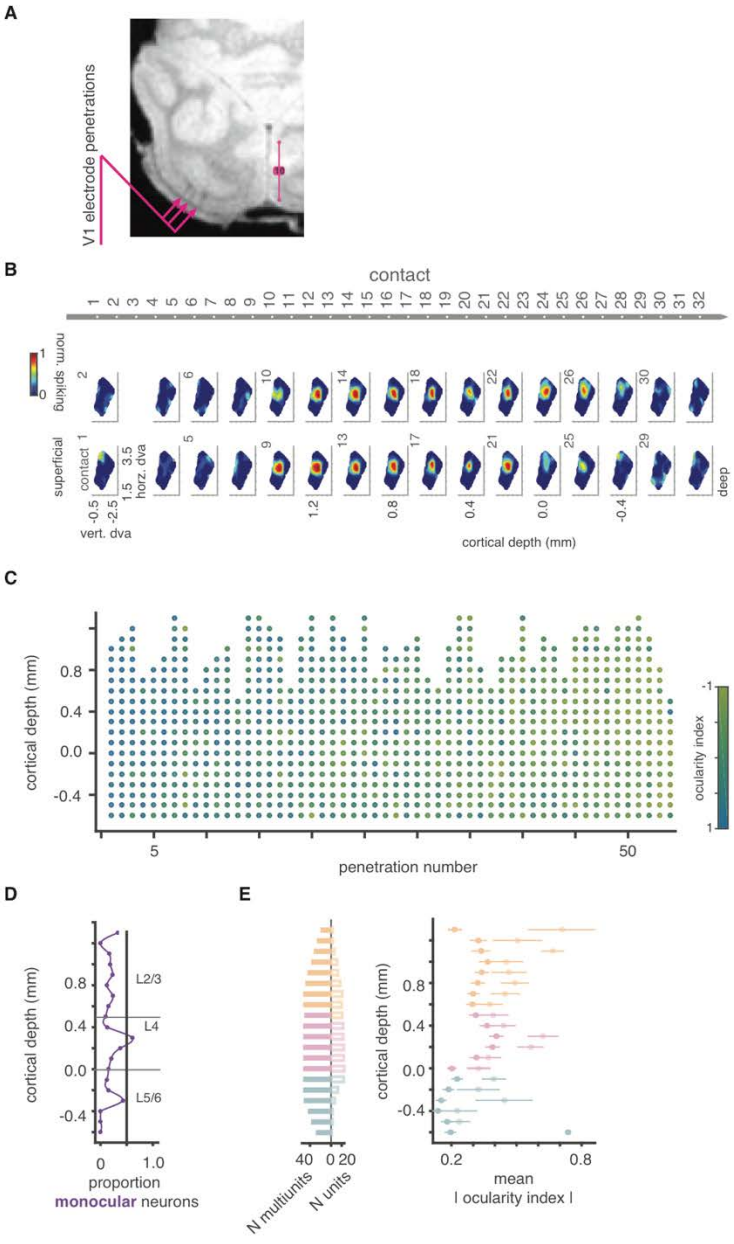
A
V1 electrode penetrations
B
contact
norm. spiking
superficial
contact
deep
horz. dva
vert. dva
cortical depth (mm)
C
cortical depth (mm)
penetration number
ocularity index
D
cortical depth (mm)
L2/3
L4
L5/6
proportion
monocular neurons
E
N multiunits
N units
cortical depth (mm)
mean
| ocularity index |

Figure S1. Laminar alignment. ***Related to Figure 1, Figure 4****.*

A Magnetic resonance image (axial slice). Arrows point to the susceptibility artifact caused by cerebrospinal fluid in the area where electrodes were located.

B Example response field matrices extracted from multiunit activity from 32 electrode contacts during a single electrode penetration of V1. Each map is Gabor-filtered, and z-score transformed.

C Ocularity indices of multiunits across cortical depth for each penetration. Penetrations are sorted from left to right, based on the mean ocularity index across units. Penetration 54 (farthest right) was excluded from all laminar analyses with 0.1 mm resolution because it included units that strongly preferred one eye or the other eye as well as an atypical CSD response, suggesting that the penetration was oblique relative to the surface of cortex.

D Proportion of monocular neurons across the cortical depth based on total population (n = 64 monocular neurons, n = 290 total neurons).

E Number of multiunits and number of single neurons (hollow symbols) (left) included in the computation of the mean rectified ocularity index at each cortical depth (right).

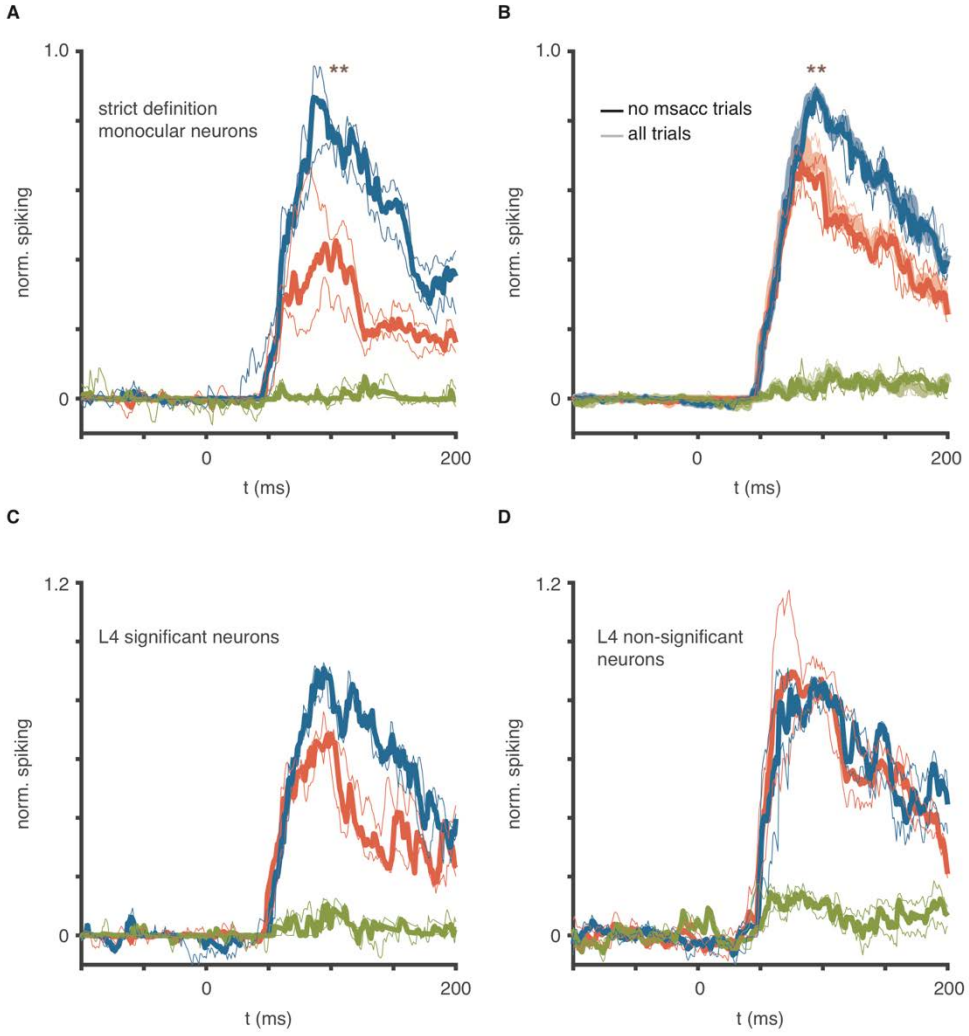
A
B
C
D
1.0
1.2
0
200
t (ms)
norm. spiking
**
strict definition
monocular neurons
no msacc trials
all trials
L4 significant neurons
L4 non-significant
neurons

Figure S2. Binocular modulation upholds with a stricter criterion for defining monocular neurons, occurs in L4 and is unrelated to microsaccades. ***Related to Figure 1 and Figure 2.***

A Median responses of monocular neurons that were deemed completely unresponsive to the non-dominant eye using a stricter criterion (N = 8). Binocular modulation is significant (two-tailed Wilcoxon signed-rank, p = 0.0078). All conventions as in **Figure 1**.

B Median responses of monocular neurons (same as **Figure 1** and **2**, N = 33) to binocular (orange), dominant eye (blue), and non-dominant eye (green) stimulation. Lighter colors represent responses using all trials. Darker colors indicate subset of trials without microsaccades. All other conventions as in **Figure 1**. Binocular modulation remains significant with all microsaccade-containing trials excluded (two-tailed Wilcoxon signed-rank, p = 0.0076).

C Median responses of L4 monocular neurons (n = 11) that show a significant difference between binocular and dominant eye stimulation based on ROC analysis ($\alpha = 0.05$). All other conventions as in **Figure 1**.

D Same as **C** for L4 monocular neurons (N = 6) that did not show a significant difference between binocular and dominant eye stimulation.

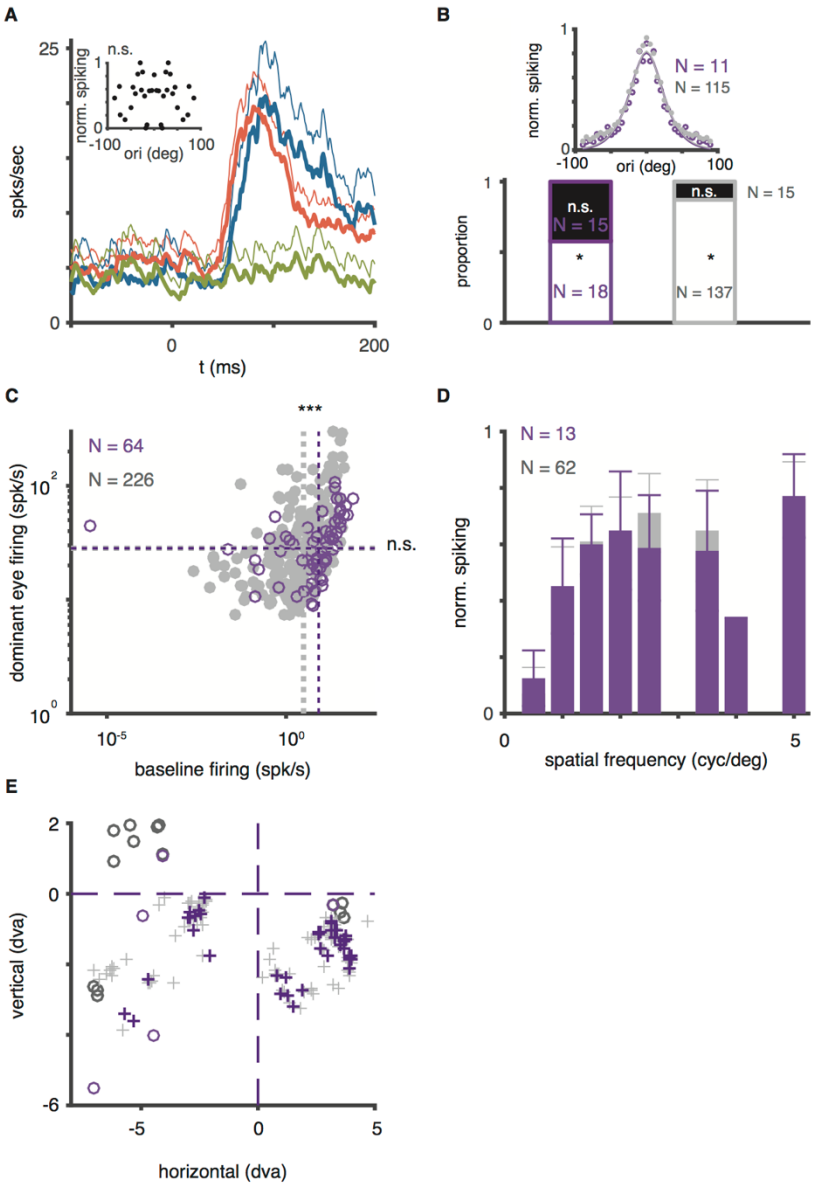
A
25
spks/sec
0
0
200
t (ms)
n.s.
norm. spiking
1
0
-100
ori (deg)
100
B
norm. spiking
1
0
-100
ori (deg)
100
N = 11
N = 115
proportion
1
0
n.s.
N = 15
*
N = 18
n.s.
N = 15
*
N = 137
C
***
N = 64
N = 226
dominant eye firing (spk/s)
10^2
10^0
n.s.
10^-5
10^0
baseline firing (spk/s)
D
1
0
N = 13
N = 62
norm. spiking
0
5
spatial frequency (cyc/deg)
E
2
0
-6
vertical (dva)
-5
0
5
horizontal (dva)

Figure S3. **Orientation tuning, spatial frequency tuning, firing rate characteristics, and RF locations of monocular and binocular V1 neurons.** ***Related to Figure 1.***

A L4 non-orientation tuned monocular neuron showing significant binocular modulation. Responses to binocular (orange), dominant eye (blue), and non-dominant eye (green) stimulation. Significance assessed via ROC analysis ($\alpha = 0.05$). Thin lines represent 95% confidence bound. Inset: Normalized responses to high contrast gratings shown at varying orientations. There was no significant effect of orientation (ANOVA, $p > 0.05$).

B Top: Mean tuning functions for monocular (purple) and binocular units (gray), using Gaussian fit. Units without a significant effect for orientation (ANOVA, $p < 0.05$) and a Gaussian fit with r^2 less than 0.5 were excluded from analysis. Bottom: Fraction of significant orientation-tuning among monocular neurons (left) and binocular neurons (right).

C Baseline firing rate versus dominant eye response for monocular and binocular neurons, respectively. Color coding as in **B**. The baseline firing rate of monocular neurons was significantly higher than that of binocular neurons (two-sample t-test, $t_{288} = 4.83$, $p = 2.22 \times 10^{-6}$).

D Monocular and binocular neurons showed the same spatial frequency tuning (multiple t-tests, all $p > 0.05$). Errors bars represent SEM.

E Receptive field center locations for monkeys I34 (circles) and monkey E48 (crosses). Color coding as in **B**.

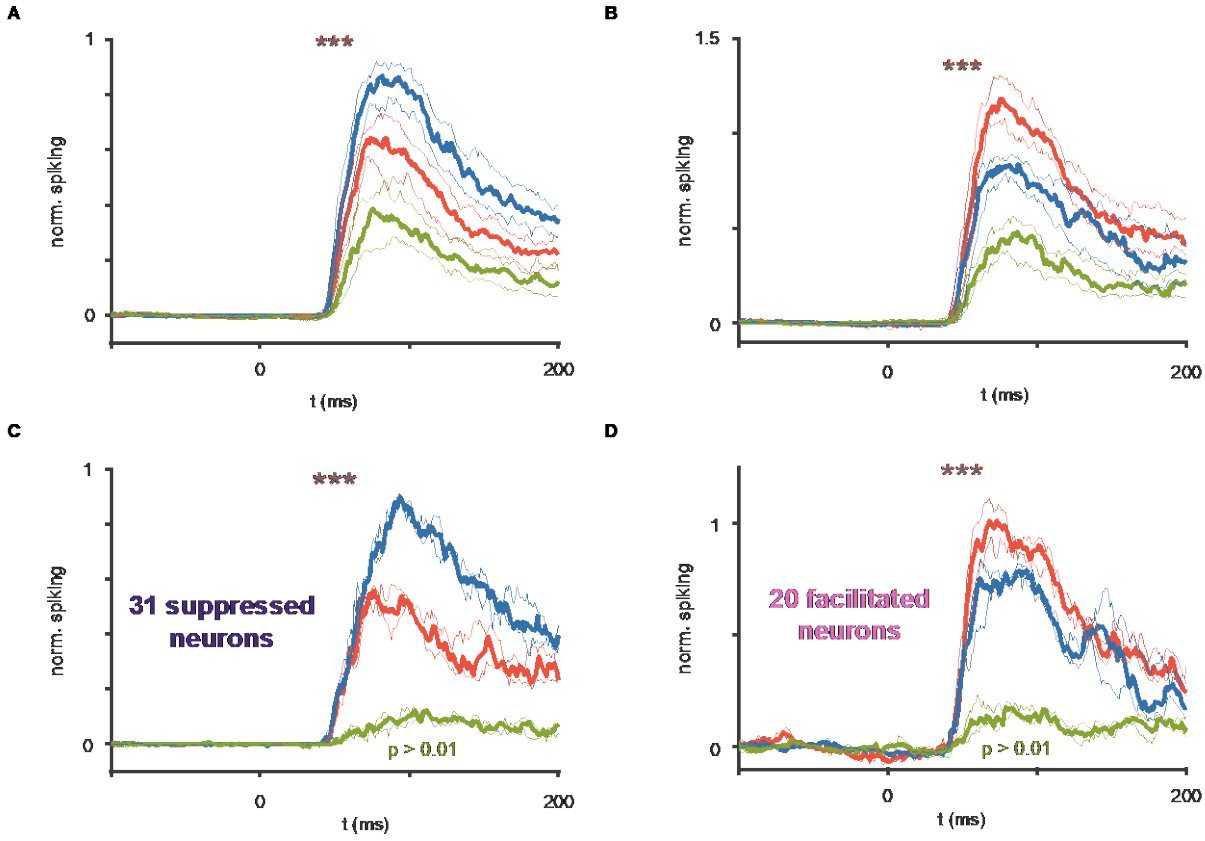
A
B
C
D
norm. spiking
t (ms)
***
31 suppressed neurons
20 facilitated neurons
p > 0.01
0
200
1
1.5

Figure S4. **Binocular modulation of binocular neurons and liberally-defined monocular neurons.** ***Related to Figure 2.***

A Population average for binocular neurons with significantly reduced responses during binocular stimulation compared to stimulation of their preferred eye alone (one-tailed Wilcoxon signed-rank, $p = 8.53 \times 10^{-10}$, N = 50). Thin lines represent 95% confidence bounds.

B Same as **A** for binocular neurons that significantly increased their responses during binocular stimulation over monocular stimulation of their preferred eye (one-tailed Wilcoxon signed-rank, $p = 5.69 \times 10^{-11}$, N = 55).

C Same as **A** for more liberally-defined monocular neurons that had a non-significant response to the non-dominant eye at $\alpha = 0.01$ (binocular versus dominant eye response, one-tailed Wilcoxon signed-rank, $p = 6.17 \times 10^{-7}$, N = 31).

D Same as **C** for more liberally-defined, facilitated monocular neurons (one-tailed Wilcoxon signed-rank, $p = 4.78 \times 10^{-5}$, N = 20).

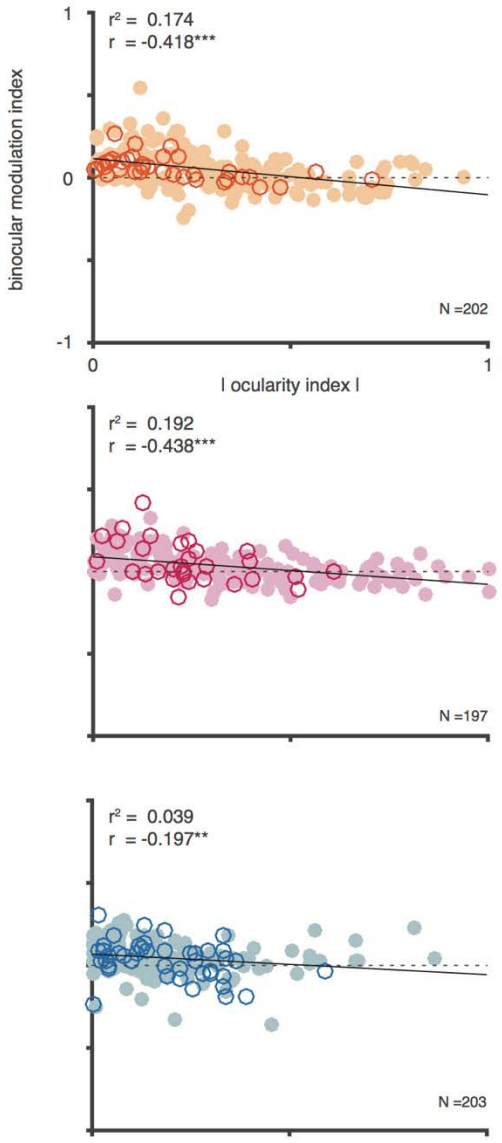
r² = 0.174
r = -0.418***
N =202
binocular modulation index
1
0
-1
0
1
l ocularity index l
r² = 0.192
r = -0.438***
N =197
r² = 0.039
r = -0.197**
N =203

Figure S5. Ocular Dominance Correlates with Binocular Modulation. ***Related to Figure 4.***

Rectified ocularity index versus binocular modulation index for multiunits in L2/3, L4, and L5/6. Hollow circles represent multiunits from monkey I34. Higher ocularity indices indicate greater preference for one eye over another. Lower binocular modulation indices indicate greater degree of suppression during binocular stimulation. The solid black line represents a linear regression using least-squares for each the supragranular ($p = 6.20 \times 10^{-10}$), granular ($p = 1.9 \times 10^{-10}$), and infragranular compartments ($p = 0.005$). The dashed line indicates the expected relationship if there were no systematic response differences between a monocular neuron's preference for one eye and its binocular modulation.

Table S1. Number of neurons used for computing the contrast response functions shown in Figure 2. ***Related to Figure 4.***

	dominant eye Michelson contrast	0.0	0.2 – 0.3	0.45 – 0.5	0.8 – 1.0
suppressed group	monocular conditions	n/a	16	16	23
	binocular conditions	23	15	16	23
facilitated group	monocular conditions	n/a	5	6	10
	binocular conditions	10	4	4	10